Ocean Engineering 209 (2020) 107501

Contents lists available at ScienceDirect

Ocean Engineering

journal homepage: www.elsevier.com/locate/oceaneng

Cross-flow vibrations of two identical elastically mounted cylinders in tandem arrangement using wind tunnel experiment

Zhongming Hu [a], Jiasong Wang [a,b,c,*], Yuankun Sun [a]

[a] School of Naval Architecture, Ocean and Civil Engineering, Shanghai Jiao Tong University, Shanghai, 200240, China
[b] State Key Laboratory of Ocean Engineering, Shanghai Jiao Tong University, Shanghai, 200240, China
[c] MOE Key Laboratory of Hydrodynamics, Shanghai Jiao Tong University, Shanghai, 200240, China

ARTICLE INFO

Keywords:
Cross-flow vibration
Flow-structure interactions
Wind tunnel experiment
Tandem arrangement
Hysteresis

ABSTRACT

In this paper, cross-flow vibrations of two identical elastically mounted circular cylinders in tandem arrangement have been investigated in a wind channel at Reynolds number $Re = 4000–42000$. The spacing ratios S/D are from 1.2 to 8.0. The vibration amplitude, oscillation frequency f_o and vortex shedding frequency f_s are investigated. Based on the vibration characteristics, three regimes can be classified. In Regime I ($S/D \leq 1.5$), the upstream cylinder experiences galloping vibration, while the downstream cylinder undergoes fluctuating with multiple peaks; In Regime II ($1.5 < S/D \leq 3.0$), two separated vibration regions can be detected for both cylinders. In Regime III ($3.0 < S/D \leq 8.0$), the upstream cylinder presents a typical vortex-induced vibration (VIV), while the downstream cylinder displays two regions including a VIV and wake-induced galloping (WIG). A hysteresis phenomenon can be observed at $S/D = 1.5$ and 2.0 for different initial test conditions ('from rest' and 'increasing velocity'). The effect of the initial states (fixed or elastically mounted) of the neighbouring cylinder on the other cylinder is also significant. The f_s can be locked to the multiple harmonics of natural frequency f_n, while the dominant f_o can only be locked to the first harmonic of f_n.

1. Introduction

Vortex-induced vibration (VIV) of an isolated circular cylinder free to vibrate in the cross-flow (CF) direction has been made great achievements in the past decades. A number of significant phenomena and conclusions have been revealed by previous investigators. One can refer to the reviews by Bearman (1984), Parkinson (1989), Blevins (1990), Sarpkaya (2004) and Williamson and Govardhan (2004). However, there are many multiple cylindrical structures applied in practical engineering, such as risers, offshore platforms, tubes of heat exchangers, bridge cables, high voltage transmission lines, etc. As the most basic and simplest configuration of multiple cylindrical structures, the studies on a two-cylinder system are of fundamental and practical significance.

Early experiments, mainly focusing on the fluid flow of structures, have been performed many on two stationary cylinders. Zdravkovich (1987, 1988) classified the flow pattern of two staggered arrangement cylinders into three regimes: 'no-interference' regime where the downstream cylinder is far apart from the upstream one, there is no effect on each other just like a single cylinder; 'proximity interference' is the region where the downstream cylinder is close enough to suffer interference from the flow deflected by the upstream cylinder, but is not immersed in its wake. Finally, when the downstream cylinder is immersed in the wake of the upstream cylinder partially or completely, it is called the 'wake interference'. Igarashi (1981) carried out experimental investigations on the characteristics of the flow around two tandem stationary cylinders. He presented a detailed classification of the flow structure depended on spacing ratios S/D (from 1.03D to 5D) and Re (from 8.7×10^3 to 5.2×10^4). Zhou and Yiu (2006) performed a series of similar experiments, the flow structure can be generally classified into three regimes depended on S/D and Re: (I) 'Extended-body regime', in this regime the two cylinders are sufficiently close that the shear layers generated from upstream cylinder overshoot downstream cylinder, just like a single body; (II) 'Reattached regime', where the separated shear layers can reattach on the downstream cylinder; (III) 'Co-shedding regime', the distance between the cylinders is sufficiently far apart that the separated shear layers from the upstream cylinder roll up, and vortex streets can be formed in the gap and behind the rear cylinder. Some related reviews on this topic can be found in Zdravkovich (1988), Sumner (2010), Zhou and Alam (2016).

Flow-induced vibration (FIV) of one-fixed-one-free tandem

* Corresponding author. School of Naval Architecture, Ocean and Civil Engineering, Shanghai Jiao Tong University, Shanghai, 200240, China.
E-mail address: jswang@sjtu.edu.cn (J. Wang).

https://doi.org/10.1016/j.oceaneng.2020.107501
Received 9 January 2020; Received in revised form 5 May 2020; Accepted 6 May 2020
Available online 28 May 2020

Nomenclature

y	Vibration displacement
D	Cylinder diameter
S	Center-to-center spacing between two cylinders
S/D	Spacing ratio
U	Free stream velocity
l	Cylinder length
A	Vibration amplitude
A_{max}	Maximum vibration amplitude
A/D	Non-dimensional vibration amplitude
A_{max}/D	Non-dimensional maximum vibration amplitude
A_u^n	Non-dimensional vibration amplitude of upstream cylinder
A_d^n	Non-dimensional vibration amplitude of downstream cylinder
ϕ	Phase angle between the two vibration cylinders
f_n	Natural frequency
f_o	Oscillation frequency
f_s	Vortex shedding frequency
ζ	Damping ratio
ν	Kinematic viscosity of the fluid
ρ	Fluid density
Re	Reynolds number ($Re=UD/\nu$)
U_r	Reduced velocity ($U_r = U/f_n D$)
St	Strouhal number ($St = f_s D/U$)
m_a	The added mass in still fluid
m^*	Mass ratio ($m^* = 4m/(\pi\rho D^2 l)$)
$m^*\zeta$	Mass-damping ratio

arrangement cylinders has been studied by a large number of investigators, and some excellent findings have been achieved. In this regime, the upstream cylinder is fixed and the rear one can freely vibrate in the CF direction. Bokaian and Geoola (1984a) investigated the FIV of two rigid cylinders arranged in tandem by performing water channel experiments (mass ratio $m^* = 8.4$, damping ratio $\zeta = 0.013$). It was found that, depending on S/D, m^* and ζ, the downstream cylinder exhibited four dynamic regimes: galloping only, vortex resonance (VR) only, separated VR and galloping, and combined VR and galloping. Brika and Laneville (1999) carried out experiment to investigate the vibration response of a flexible cylinder in the wake of a stationary one using wind tunnel under the conditions of $Re = 5000$–27000, $S/D = 6.5$–24.5, $m^* = 821$, $\zeta = 0.00008$. The spacing ratio, S/D, presented a significant influence on the dynamic response of the rear flexible cylinder. With the increasing of S/D, the vibration amplitude decreased and it could be inferred that the response would resemble that of an isolated cylinder when S/D was larger than a critical value. Hover and Triantafyllou (2001) performed an experiment with an elastically mounted downstream cylinder towed behind an identical fixed one for 4.75 diameters in water, in their experiment $Re = 30000$, $m^* = 3.0$ and $\zeta = 0.04$. The vibration amplitude increased monotonically as a function of reduced velocity U_r and reached the maximum amplitude $A_{max}/D = 1.9$ at $U_r = 17$. Assi et al. (2010) investigated the mechanism of wake-induced vibrations (WIV) of two cylinders in a tandem arrangement ($m^* = 2.6$ and $\zeta = 0.007$). They suggested that WIV could be attributed to the unsteady vortex-structure interactions between the downstream cylinder and the vortex shedding from the upstream body. A combined VIV and WIV can be observed in the experiment at $S/D \leq 6.0$, while with the increasing of S/D, the vibration response tending to a single cylinder. Qin et al. (2017) experimental investigated the FIV of a elastically mounted cylinder with larger diameter D placed behind a fixed one with a smaller diameter d, where the $d/D = 0.2$–1.0 and $S/D = 1.0$–5.5.They noted that the large-scale vibration is more likely to occur at smaller d/D as S/D increases.

The FIV characteristics become more complicated when the two cylinders can both vibrate freely. Kim et al. (2009) carried out a series of experiments to investigate the free vibration response of two rigid cylinders in CF using wind tunnel. The system had a mass-damping ratio $m^*\zeta$ of 0.65, and S/D was from 1.1 to 4.2 companied with reduced velocity $U_r = 1.5$–26. Depending on S/D and vibration characteristics, different amplitude response regimes can be observed. The vibration was absent at $1.1 \leq S/D < 1.2$ and $3.0 \leq S/D < 3.7$. Both cylinders suffered violent galloping response at $1.2 \leq S/D < 1.6$ for $U_r > 6$. At $1.6 \leq S/D < 3.0$, the convergent vibration could be observed around $U_r \approx 6.7$. At $S/D \geq 3.7$, each cylinder resembled a single cylinder since the spacing ratio S/D is far enough. However, the vortex shedding frequency was not examined in their experiment. Huear-Huarte and Bearman (2011) performed experiments on the dynamic responses of two flexible cylinders in tandem arrangement using water tunnel ($m^*\zeta = 0.043$, $S/D = 2.0$–4.0). The upstream cylinder presented larger vibration than the downstream cylinder at $S/D = 2.0$–2.5 for $U_r = 4$–9. While for large spacing ratio ($S/D = 3.0$–4.0), the downstream cylinder exhibited non-classical VIV with violent vibration at high U_r. Huear-Huarte and Gharib (2011) further studied the responses at $S/D = 4.0$–8.0 (far wake interference). It can be demonstrated that the upstream cylinder displayed a typical VIV behavior similar to a single cylinder, while the rear one presented WIV with large amplitude even though the U_r beyond the classical lock-in region when the S/D was large enough. Huang and Herfjord (2013) investigated the FIV of two elastically mounted rigid cylinders in staggered and tandem arrangement. They found that the motion trajectories of the downstream cylinder were depended on whether the two cylinders were in tandem or staggered arrangement. They also discussed the influence of the local reduced velocity for downstream cylinder on the its own vibration response. The local reduced velocity was not measured but estimated by a wake velocity model. By using a towing tank, Armin et al. (2018) performed experiments on the responses of two tandem elastically mounted cylinders with Reynolds numbers ranging from 8.7×10^3 to 5.2×10^4. The cylinders can vibrate in both in-line (IL) and cross-flow (CF) direction and the spacing ratios S/D were set from 3.5D to 20D. They found that, for all spacing ratios, the upstream cylinder undergone VIV response which was similar to the single cylinder. However, the downstream cylinder was significantly influenced by the front one and the S/D. Another important phenomenon was that the two cylinders vibrated at different frequencies which was contrary to the previous conclusions on the fixed one. Qin et al. (2018) carried out a series of experiments to study the CF vibration of two tandem cylinders with six different natural frequencies (0.6, 0.8, 1.0, 1.2, 1.4, 1.6). Two spacing ratios $S/D = 1.5$, 2.0 were chosen to analysis. Base on the natural frequency ratios and reduced velocity, three regimes can be distinguished: no lock-in, vortex excitation, galloping regimes. Xu et al. (2019) presented experimental results of two elastically mounted tandem cylinders in CF direction by using a water tunnel with $m^*\zeta = 0.027$ at $Re = 28600$-11400. Four spacing ratios $S/D = 1.57$, 2.57, 3.57, 4.57 were chosen in their experiment. Results indicated that the vibration amplitude, frequency response and total fluid force coefficient of upstream cylinder were similar to those of an isolated cylinder at higher spacing ratio ($S/D = 2.57$, 3.57, 4.57) for $U_r < 12$. While at $S/D = 1.57$, it presented galloping response with a divergent-amplitude vibration. The downstream cylinder experienced VIV-like response with wider lock-in region for all the spacing ratios tested in their experiment.

Except experimental investigations on the FIV of two elastically mounted tandem cylinders, there exist a number of numerical simulations focusing on this topic as well. Most of them carried out at low Re, such as Mittal and Kumar (2001), Papaioannou et al. (2008), Prasanth and Mittal (2009), Borazjani and Sotiropoulos (2009), Wang et al.

(2017). Papaioannou et al. (2008) studied the effect of S/D on the vibration response of two tandem cylinders in two degrees of freedom at $Re = 160$ for $m^*\zeta = 0.127$. Three spacing ratios, $S/D = 2.5$, 3.5 and 5, were selected. It can be observed that the VIV region of the upstream cylinder was sensitive to S/D, and it became wider at smaller S/D. Attributing to the shielding effect, the response curves of the rear were shifted toward higher values of U_r than those of upstream cylinder for all examined S/D. Borazjani and Sotiropoulos (2009) focused on the FIV of two tandem cylinders with one and two degrees of freedom in the near wake interference region ($S/D = 1.5$) at $Re = 200$. Two vibration situations could be illustrated. At low U_r, the vibration amplitude of the upstream cylinder was greater than that of the rear one. While, once U_r increased to a critical value, the downstream cylinder would undergo violent vibration with larger amplitude than that of the front one. Wang et al. (2017) investigated the VIV of two tandem flexible cylinders using a two-way fluid-structure interaction (FSI) method. The simulations were performed for $Re = 500$ at three spacing ratios ($S/D = 2.5$, 3.5, 5.0) with $m^* = 10$ and $\zeta = 0$. It was observed that the upstream cylinder presented a typical VIV response for all S/D examined. The downstream cylinder was also similar to the typical VIV at small spacing ratios. While when the spacing was large enough that the shear layers from the upstream cylinder can roll up in the gap, it experienced WIV with a large-amplitude at high U_r. Lin et al. (2020) numerically investigated the FIV of two tandem elastically mounted cylinders at subcritical Reynolds numbers with $S/D = 4.0$. They found that the variation of the vortex shedding frequency of the upstream cylinder had a weak influence on the amplitude and dominant frequency of the rear one. And the FIV characteristics of the downstream cylinder presented a significant dependence on the Reynolds number.

FIV of two elastically mounted tandem arrangement cylinders is influenced by a number of parameters, such as spacing ratio S/D, mass-damping ratio $m^*\zeta$, Reynolds number Re and initial test conditions used in the experiment. Therefore, despite performing a number of experimental and numerical studies in the past on this field, some issues are still needed to be conducted to have a better understanding. For example, what are the responses including vibration amplitude, oscillation frequency and vortex shedding frequency with a mass-damping ratio $m^*\zeta = 0.2$ in air, which is usually larger than that in water? How do the initial test conditions ('from rest' and 'increasing velocity') used in the experiment affect the vibration response and whether there existing a hysteresis phenomenon? What is the underlying mechanism of hysteresis phenomenon and why it only occurs at some small S/D? How does the initial state of the neighbouring cylinder (fixed or elastically mounted) affect the amplitude response of the other one? Here, this paper aims to address the above issues. The spacing ratio, S/D varied from 1.2 to 8.0 from proximal to far wake. Two initial test conditions, 'from rest' and 'increasing velocity', are used in the experiment. (I) 'from rest' regime: the cylinder is released from rest at any given U_r with human intervention. (II) 'increasing velocity' regime: the cylinder starts to vibrate at a steady-state amplitude produced by the previous and continuously increasing U_r without outside interference.

The paper is organized as follows. In section 2, the experimental setup is described. Experimental methodology validation and preliminary results for a single cylinder are given in section 3. Section 4 presents the results and discussions for the two identical elastically mounted cylinders. The conclusion of the work is shown in section 5.

2. Experimental details

The experiments were carried out in a low-speed wind tunnel with a test section of 0.6 m in width, 0.6 m in height and 2.0 m in length. The turbulent strength scale is less than 0.2%. Further details of the wind tunnel were introduced by Gu et al. (2012), Sui et al. (2016) and Liang et al. (2018).

Two hollow cylinders are horizontally mounted in tandem arrangement (Fig. 1 a) in the test section with outer diameter D = 50 mm and inner diameter d = 48 mm. The length of each cylinder is 540 mm with aspect ratio of 10.8 and blockage of 7.5% approximately. The cylinders are made of Plexiglass to keep low mass and excellent smoothness. Each cylinder was supported by four spiral springs made of stainless steel respectively at each side (eight spiral springs used in total) and can only vibrate in the CF direction (Fig. 1 b). The free stream velocity was in the range of 1.2 m/s - 12.5 m/s in the current test with the corresponding Reynolds number = 4000–42000 and $U_r = 2.4$–25.0. The mass ratios m^* of the upstream and downstream cylinders are both 268.9. In order to measure the damping ratios ζ and natural frequency f_n, a series of free decay experiments were conducted in still air. That is the cylinder is excited to oscillate freely by giving an initial displacement. The free decay duration curve is presented in Fig. 2 a. The value of damping ratios ζ is estimated to be 0.00075, and as a result, the combined mass-damping ratio $m^*\zeta$ can be yielded 0.20. The value of natural frequency f_n is 10.05 Hz which can be determined by fast Fourier transform (FFT) on the basis of free decay experimental displacement data (Fig. 2 b.).

The displacement responses y of the upstream and downstream cylinders were measured utilizing a laser sensor (IL-300, Keyence) after the vibrations stabilizes. The oscillation frequencies of the cylinders can be obtained via FFT based on the measured displacement data. The streamwise fluctuating velocities u' were measured through a hot wire probe named HW (Dantec 55p11), which was placed behind the downstream cylinder as shown in Fig. 1 b. The horizontal and vertical distances between the hot wire probe and downstream cylinder remain unchanged (4D in horizontal and 1D in vertical), though S/D varying. The sampling rate is set to be 1024Hz and the majority sampling duration used for calculation is 20 s when the cylinder achieves the stable vibration. For few special cases which fail to achieve a steady state (beating phenomenon shown in Fig. 7 d), longer time will be used.

3. Experimental methodology validation and preliminary results

To verify the experimental methodology and ensure the characteristics of the upstream and downstream cylinders being identical, separated tests for the two cylinders were preliminarily performed. The non-dimensional amplitude responses A/D of present experimental results versus reduced velocity U_r together with the past outstanding researches for comparison are shown in Fig. 3. And Fig. 3 b plots the vortex shedding frequencies f_s for the separated upstream and downstream cylinders at present study particularly. The amplitude A is calculated by multiplying the root-mean-square (r.m.s.) value of displacement signal y by $\sqrt{2}$ when the vibration is stable. As shown in Fig. 3 a and b, the vibration amplitude responses and vortex shedding frequency ratios are nearly the same implying both cylinders are strictly identical to each other. Two typical branches, initial and lower branches can be observed. The VIV region (lock-in region) occurs at around $U_r = 4.6$–8.7 associated with $f_s/f_n = 1$ and the maximum value of vibration amplitude occurs at around $U_r = 6.0$. Once beyond the range, the vibration is weak and f_s/f_n almost follows $St \approx 0.19$ line which is very close to 0.2 when the cylinder is stationary. These characteristics are in good agreement to the previous results in wind tunnel with large $m^*\zeta$, such as Feng (1968), Sui et al. (2016) and Liang et al. (2018). While, an upper branch with very large amplitude is presented in the experiments by Armin et al. (2018) and Huang and Herfjord (2013) for small $m^*\zeta$ in water tunnel and the lock-in regions are also wider. This can be mainly attributed to the influence of mass-damping ratio $m^*\zeta$.

The non-dimensional maximum amplitudes (A_{max}/D) are displayed in Fig. 4 as a function of $m^*\zeta$, including several experimental data carried out by previous investigators, such as Zhou et al. (2011) and Assi et al. (2013) etc. The blue line represents a curve fitting to the results of a large number of previous researches, compiled originally by Griffin (1980), and updated after by Skop et al. (1997). As can be seen from the graph, the current result can fit the curve well, therefore the present

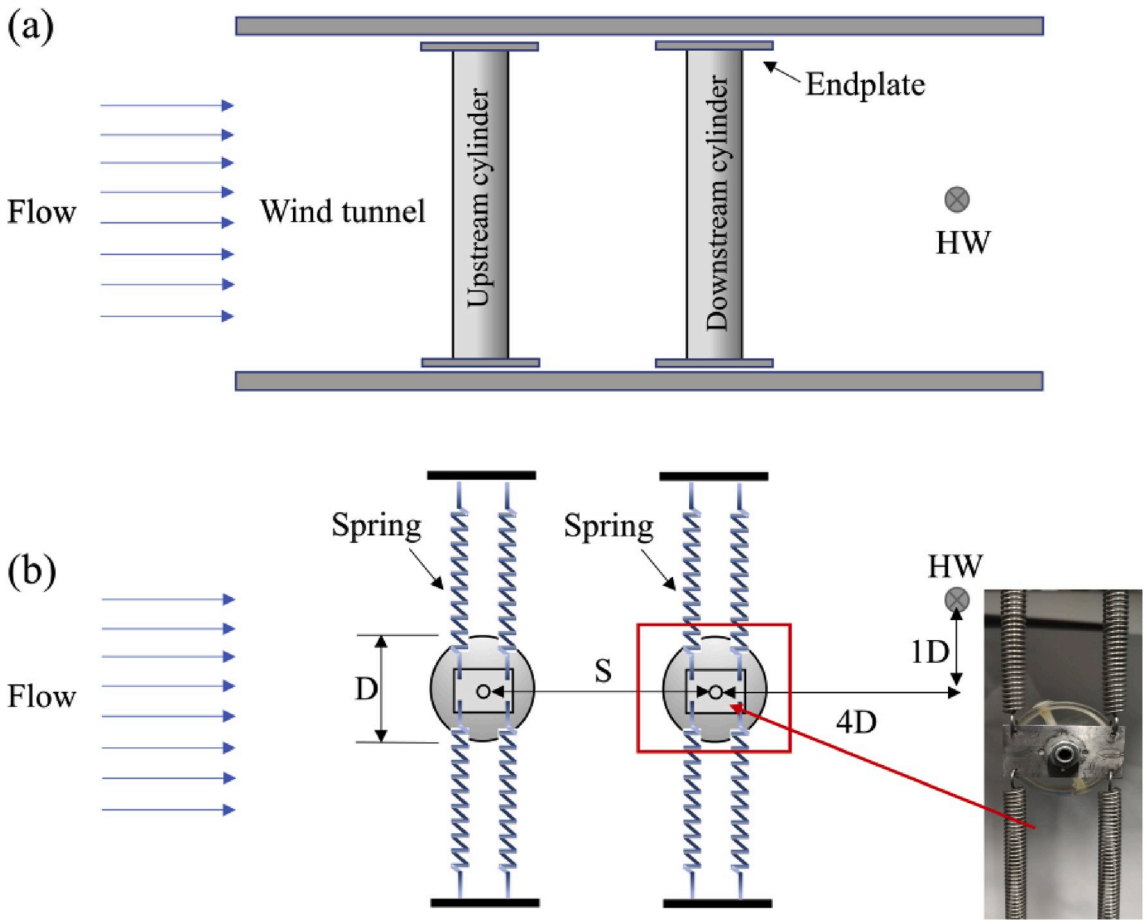

Fig. 1. Configuration of the experimental arrangement.

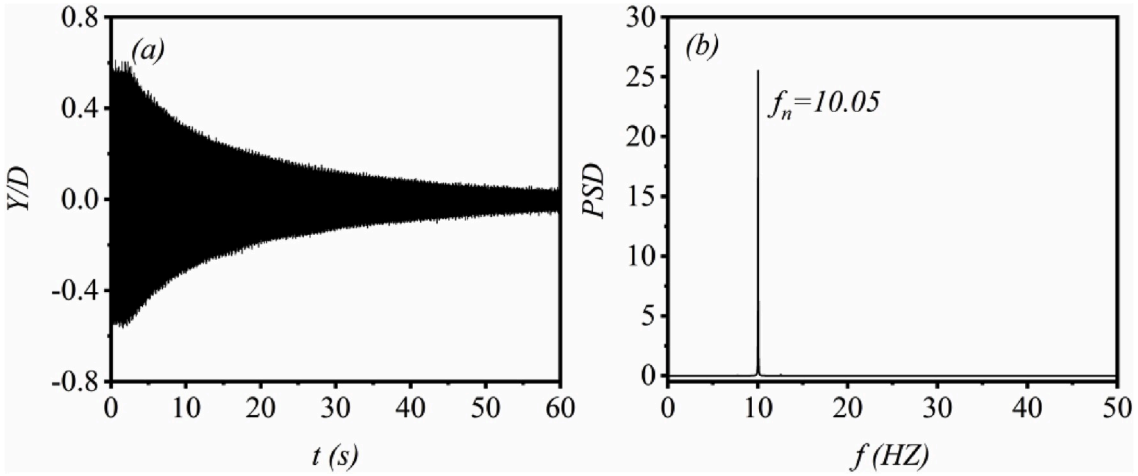

Fig. 2. (a) Decay curve of the displacement after a plucking excitation, and (b) *PSD* of the displacement signal.

method is well validated by an experiment of classical single cylinder for high $m^*\zeta$ in wind tunnel.

4. Results and discussion

The CF vibration characteristics of two elastically mounted cylinders in tandem arrangement are systematically investigated primarily under the initial condition of 'increasing velocity'. Depending on spacing ratio S/D and reduced velocity U_r, the results are presented including non-dimensional vibration amplitude A/D, oscillation frequency f_o and vortex shedding frequency f_s.

And then, the influence of initial test conditions ('from rest' and 'increasing velocity') on the vibration responses of the two cylinders and the influence of initial states (fixed or elastically mounted) of the neighbouring cylinder on the other one are studied and discussed, respectively.

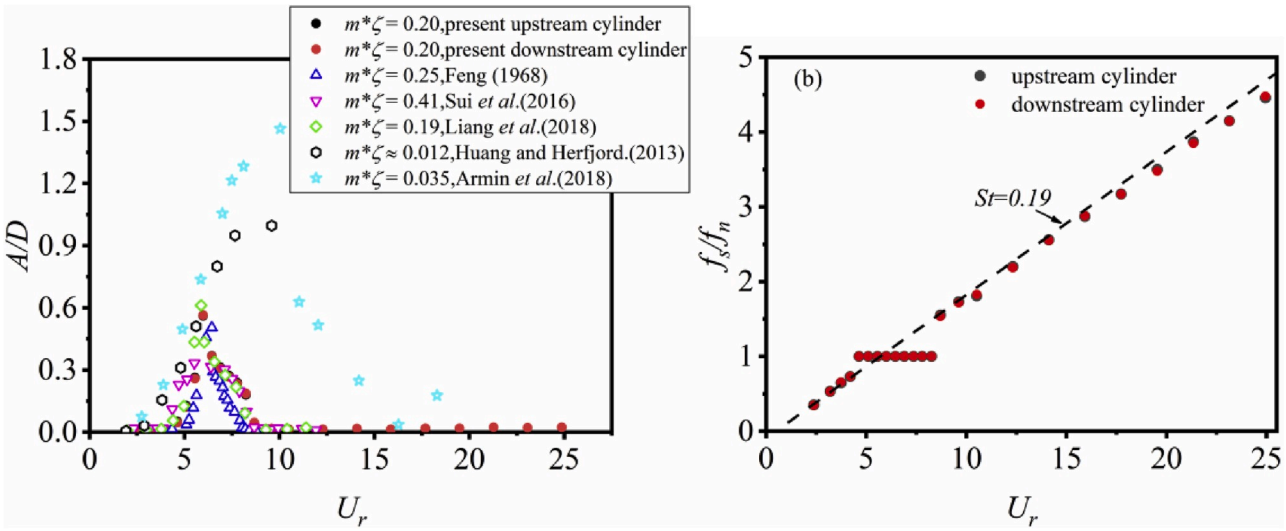

Fig. 3. Comparison of different mass-damping parameters for a single cylinder. (a) Vibration amplitude response, and (b) vortex shedding frequency response.

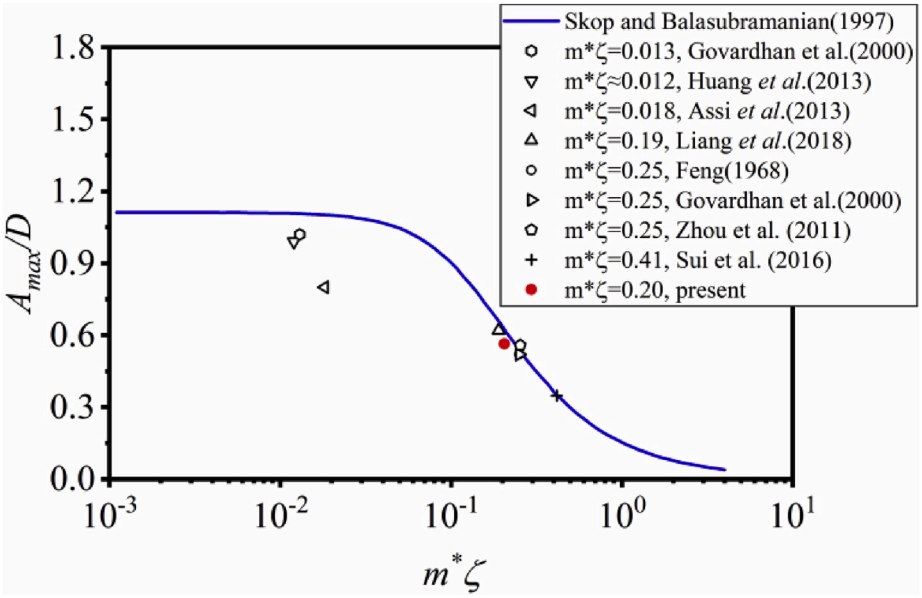

Fig. 4. Dimensionless maximum amplitude A_{max}/D versus mass-damping parameter $m^*\zeta$.

4.1. Vibration characteristics depending on S/D

Fig. 5 illustrates the non-dimensional amplitudes of the upstream (A_u^n) and downstream cylinders (A_d^n) versus U_r depending on S/D. Comparing to that of the single cylinder in Fig. 3, the vibration amplitude responses are more complicated. It is evident that the amplitudes are really sensitive to S/D and U_r. Based on the vibration characteristics of the two cylinders, three regimes can be classified.

4.1.1. Vibration characteristics in RegimeI($S/D \leq 1.5$)

In this Regime, the upstream cylinder experiences galloping vibration, while A_d^n undergoes fluctuating with multiple peaks as a function of U_r, and A_u^n is roughly greater thanA_d^n during the whole range of examined U_r. At $S/D = 1.2$ (see Fig. 5 a), both of them start to vibrate at around $U_r = 3.7$ earlier than that of the single cylinder and maintain nearly the same trend until at $U_r = 5.1$. After that, A_u^n still increases rapidly as the U_r gets larger and achieves a peak of about 1.4 at $U_r = 18.5$. Generally speaking, A_u^n is rising with the increasing of U_r indicating the occurrence of galloping vibration even though along with a slight fluctuation. Whereas, A_d^n achieves the first hump with a local peak at $U_r = 6.4$, which is very closed to the point of the maximum amplitude takes place for the single cylinder and then continues to increase rapidly and undergoes a roughly stable plateau (the second hump) with the amplitude larger than 0.9 in the region of $10.5 < U_r < 15.9$. Afterwards, A_d^n decreases abruptly, and then gradually increases again after $U_r = 18.6$, exhibiting the third hump. At $S/D = 1.09$–1.75, the galloping vibration were also observed by Bokaian and Geoola (1984b) for the upstream cylinder with a fixed downstream cylinder, the value of $m^*\zeta$ was 0.093 which is smaller than present study. At $S/D = 1.5$ (see Fig. 5 b), A_u^n increases apparently till to a local peak and then decreases, after that it remains convergent galloping vibration. The behavior of upstream cylinder is similar to that in Xu et al. (2019) at $S/D = 1.57$ and Borazjani and Sotiropoulos (2009) at $S/D = 1.5$. The A_d^n is still fluctuating along with three humps, but it is clearly that the difference between A_u^n and A_d^n becomes smaller. As observed by Kim et al. (2009), at $S/D = 1.2$–1.6, the upstream cylinder suffered a divergent galloping vibration, while the amplitude of downstream cylinder was also unstable. Note that, the maximum U_r presented in their investigation was 12 at $S/D = 1.3$ which

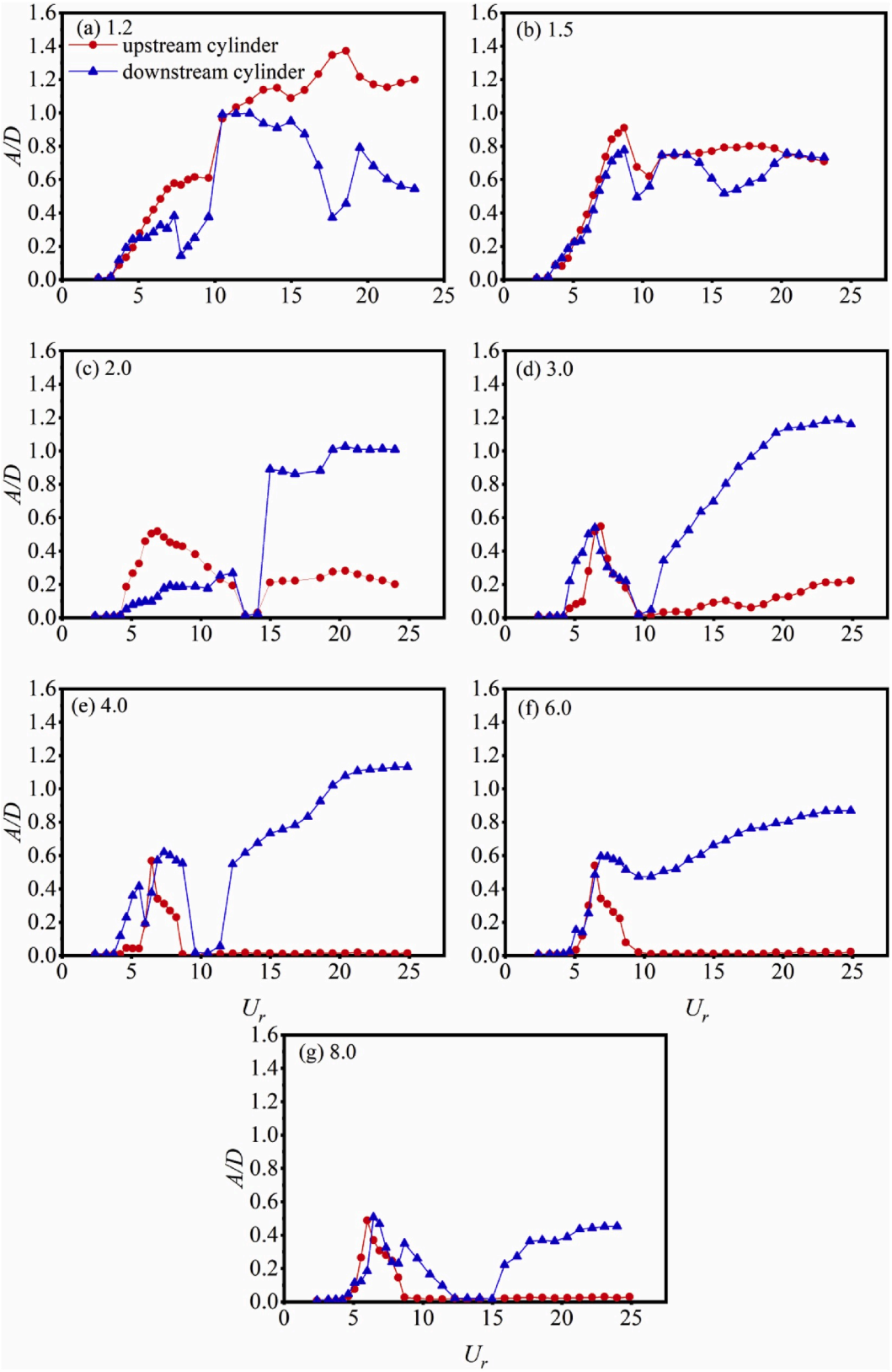

Fig. 5. Amplitude response of the two cylinders depended on S/D and U_r at (a) $S/D = 1.2$, (b) 1.5, (c) 2.0, (d) 3.0, (e) 4.0, (f) 6.0, (g) 8.0.

is smaller than the present research.

As Armin et al. (2018) reported, the phase between the vibration responses of the two cylinders played a significant role on the amplitude responses, because the vortices shedding from the upstream cylinder arrived to the rear one at random positions may amplify or minify the A_d^n. Fig. 6 shows the phase angle ϕ between the two vibration cylinders as a function of reduced velocity U_r at $S/D = 1.2$ and 1.5. It is evident that, at $S/D = 1.2$, ϕ varies unsteadily along with two discontinuities at

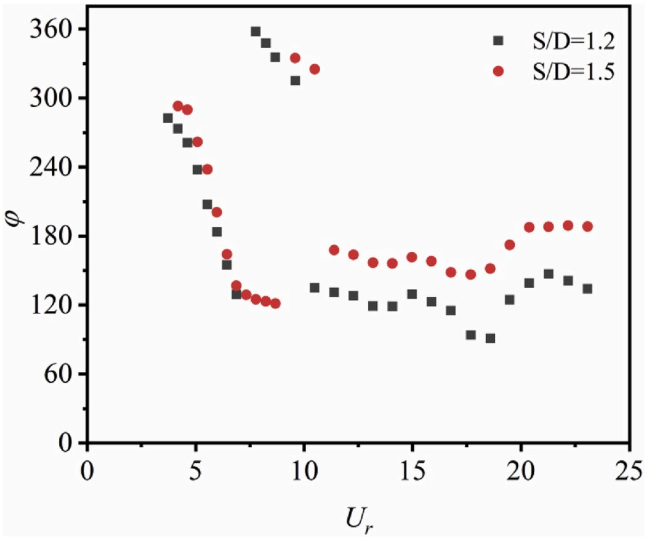

Fig. 6. Phase angle between the vibration responses of the two cylinders at $S/D = 1.2$ and 1.5.

$U_r = 6.4$ and 10.5, which are just at the points of the occurrence of the local peaks for the first and second humps of the downstream cylinder. For $U_r > 10.5$, the variation trend of ϕ is qualitatively similar to that of A_d^n. The identical characteristic can also be observed for $S/D = 1.5$ which is not repeated here for brevity.

In order to have a better understanding of the above phenomenon and also observe the process of the vibrations more clearly, Fig. 7 illustrates the instantaneous motions of the two cylinders including time history of CF displacements and their corresponding oscillation frequencies. Four representative reduced velocity, $U_r = 5.5$, 7.4, 12.3, 19.5, are chosen to present at $S/D = 1.2$. The left column (Fig. 7 a, d, g and j) displays the time history at each U_r and the middle column (Fig. 7 b, e, h and k) displays a selected 2 s of the time history when the vibration is stable. The oscillation frequencies of the corresponding signal are shown in the right column (Fig. 7 c, f, i and l). In each figure, the upper curve presents the results of upstream cylinder and the lower signifies the downstream cylinder.

At $U_r = 5.5$, during the early moments the downstream cylinder achieves a large amplitude primarily and at the same time the amplitude of the upstream cylinder accelerating increases. But after a certain time, the oscillation amplitude of the rear one decreases and finally both cylinders almost reach the stable vibration simultaneously (see in Fig. 7 a). For $U_r = 7.4$ (see in Fig. 7 d), it is evident that the two cylinders present periodically unstable motions simultaneously (beating phenomenon), implying the interference between them is strong. When U_r increases to 12.3 (see in Fig. 7 g), the cylinders can eventually achieve stable vibrations after the early tens of seconds unsteady motions. If further increasing U_r to 19.5 (see in Fig. 7 j), both cylinders are directly able to obtain the steady-state from rest without any unstable vibration during the early moments. In general, at very small U_r, the final instantaneous motions of the two cylinders are steady. While, within a certain region of U_r, they will suffer periodically unstable oscillations at last. After that, the final situations can change from periodically unstable to stable again. It should be noted that the instantaneous motions of larger spacing ratios ($S/D > 2.0$) are similar to that of $U_r = 12.3$ or 19.5 at $S/D = 1.2$ and will not be shown here for brevity.

As shown in Fig. 7 c, f, i and l, the values of the oscillation frequencies maintain unchanged with $f_o \approx 10$ Hz very close to the natural frequency at $U_r = 5.5$, 12.3 and 19.5 if the cylinders experience a final stable vibration. While, for $U_r = 7.4$, when the cylinders suffer beating phenomenon (periodically unstable oscillations), there indeed exists a very low frequency with a very small magnitude not easy to discover. In order to have a better visual presentation, Fig. 8 consisting of local amplification frequency are presented to illustrate the frequency responses at representative reduced velocity $U_r = 5.5$ (stable vibration) and $U_r = 7.4$ (beating vibration). As can be observed from Fig. 8, at $U_r = 7.4$, it is evident that the responses of upstream and downstream cylinders consist of two frequency components, one very low frequency (about 0.02) with very small magnitude and one high frequency (close to the natural frequency) with very high magnitude. While, just one distinct peak can be found at $U_r = 5.5$ when both cylinders experience stable vibrations.

The beating phenomenon is very interesting and it is necessary to further discuss this phenomenon. Similar vibrations have been frequently observed for cylinders with two degrees of freedom (CF and IL direction) in those of Mittal and Kumar (2001), Huang and Sworn, 2011, Armin et al. (2018) etc. It can also be observed by some investigators when the cylinder can only vibrate in CF direction in those of Borazjani and Sotiropoulos (2009) and Khalak and Williamson (1999). Borazjani and Sotiropoulos (2009) focused on the FIV of two tandem cylinders (in CF direction) at $S/D = 1.5$ with $Re = 200$. The beating phenomenon can be observed at $U_r = 4$, while at other U_r the vibration can achieve a stable state. But they did not explain this phenomenon. In Khalak and Williamson (1999), they found that the phase angle ϕ 'slips' periodically through 360° as a function of time when the beating phenomenon occurred ('quasi-periodic' as defined in their paper). While, it remained close to an approximately constant value without the 'slips' through 360° when the vibration is approximately periodically stable ('periodic' as defined in their paper).

The phase angles ϕ of the displacement responses of the two cylinders versus time are calculated by using the Hilbert transform as shown in Fig. 9. It is evident that the phase angle ϕ, as in the definition of Khalak and Williamson (1999), changes periodically through 360° which is associated with beating phenomenon. But for the stable vibrations, the phase angles remain close to an approximately constant value without the 'slips' through 360°. Therefore, the beating phenomenon can be attributed to the unstable phase angle jump between the two cylinders.

The shedding frequency ratios f_s/f_n for downstream cylinder at $S/D = 1.2$ and 1.5 are depicted in Fig. 10 (a and b), respectively. In the f_s/f_n curve, a change from blue to red stands for dominant peaks of normalized power spectral density (PSD), the brighter means the higher power density. As can be seen in Fig. 10 a ($S/D = 1.2$), the value of f_s/f_n is smaller than 1.0 and almost follows $St = 0.25$ line for $U_r < 3.7$ before the onset of vibration. This is similar to but larger than the stationary cylinder (about 0.2), the result is consistent with the experimental results of Igarashi (1981) and Xu et al. (2004). In the region of $3.7 \le U_r \le 6.9$, f_s/f_n jumps to and maintains 1.0, where the amplitude response of the downstream cylinder experiences a hump and achieves a local peak, implying the occurrence of VIV. For $U_r > 6.9$, the vortex shedding frequency f_s can be locked to multiple harmonics of natural frequency f_n. The multiple harmonics usually indicate a violent vibration with complicated vortex shedding mode, for example 2S+2P mode which have been observed by Qin et al. (2017) or T + S mode by Chen et al. (2018) when galloping vibration takes place. On the other hand, the dominant value of f_s/f_n changes with the increasing of U_r implying the transition of vortex shedding mode may come up. For example, all of the first, second and third harmonics occur predominantly in the region of $11.1 < U_r < 14.4$, suggesting a kind of vortex shedding mode. While the third harmonic frequency presents predominantly at $U_r > 20.2$, may imply the dominant status of another vortex shedding mode. Similarly, at $S/D = 1.5$ (Fig. 10 b), the shedding frequency ratio f_s/f_n also changes distinctly with U_r. Specifically speaking, the f_s is predominantly locked to the first harmonic of f_n for $3.7 \le U_r \le 10.5$, the first and second harmonic for $10.5 < U_r \le 17.2$, the first and third harmonic for $17.2 < U_r \le 19.4$ and the third harmonic for $U_r > 19.4$. To present the variation of PSD more clearly, three representative reduced velocity, $U_r = 4.2$, 10.5, 21.3 at $S/D = 1.2$, are chosen. The transform of power intensity for

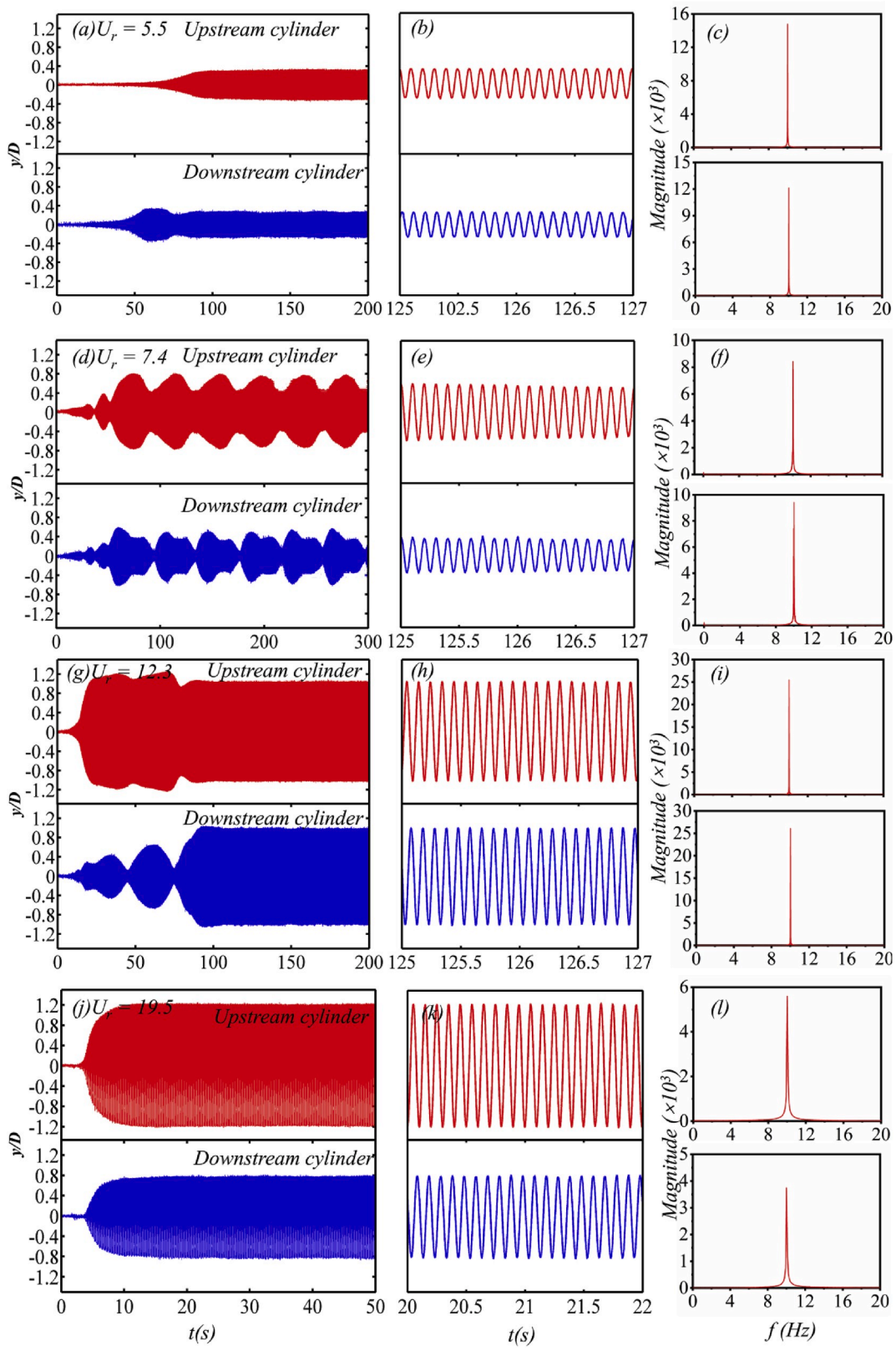

Fig. 7. Instantaneous motions and corresponding oscillation frequencies of the two cylinders at $S/D = 1.2$ for $U_r = 5.5$, 7.4, 12.3, 19.5.

different U_r can be displayed in Fig. 11. In Fig. 11 a ($U_r = 4.2$), only a first harmonic can be observed suggesting a 2S mode, while at $U_r = 21.3$ the third harmonic frequency presents predominantly indicating a complicated vortex mode. Therefore, this is in consistent with that presented in Fig. 10.

4.1.2. Vibration characteristics in RegimeII(1.5 < S/D ≤ 3.0)

Regime II is characterized by two separated vibration regions for both upstream and downstream cylinders as shown in Fig. 5 c. In the first region (at small U_r),$A_u^n$is greater thanA_d^n, while in the second region (U_r exceed a certain value), $A_u^n$is smaller thanA_d^n. At $S/D = 2.0$,A_u^nsuffers a

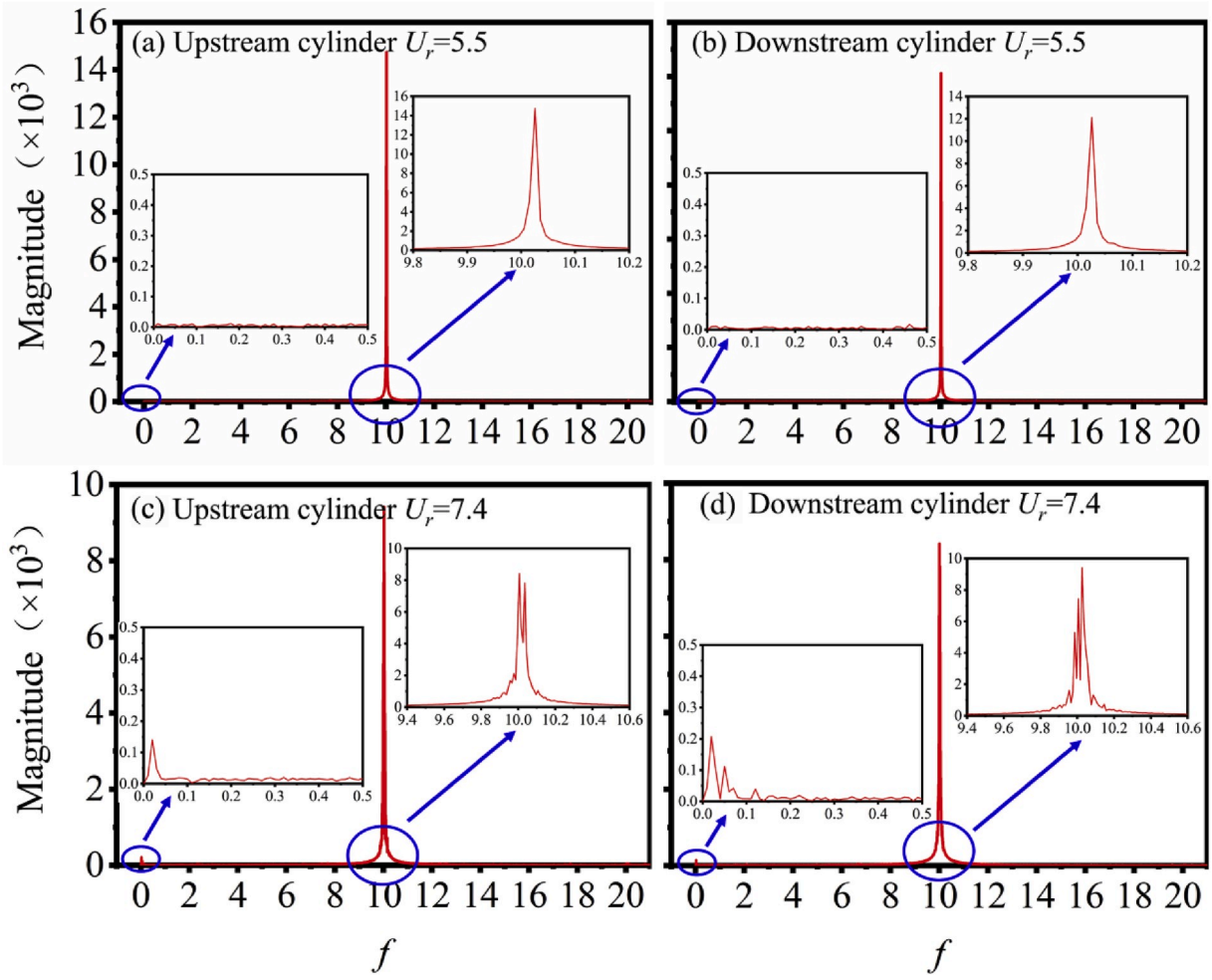

Fig. 8. Frequency response of the upstream and downstream cylinder at $S/D = 1.2$ for (a) and (b) $U_r = 5.5$, (c) and (d) 7.4.

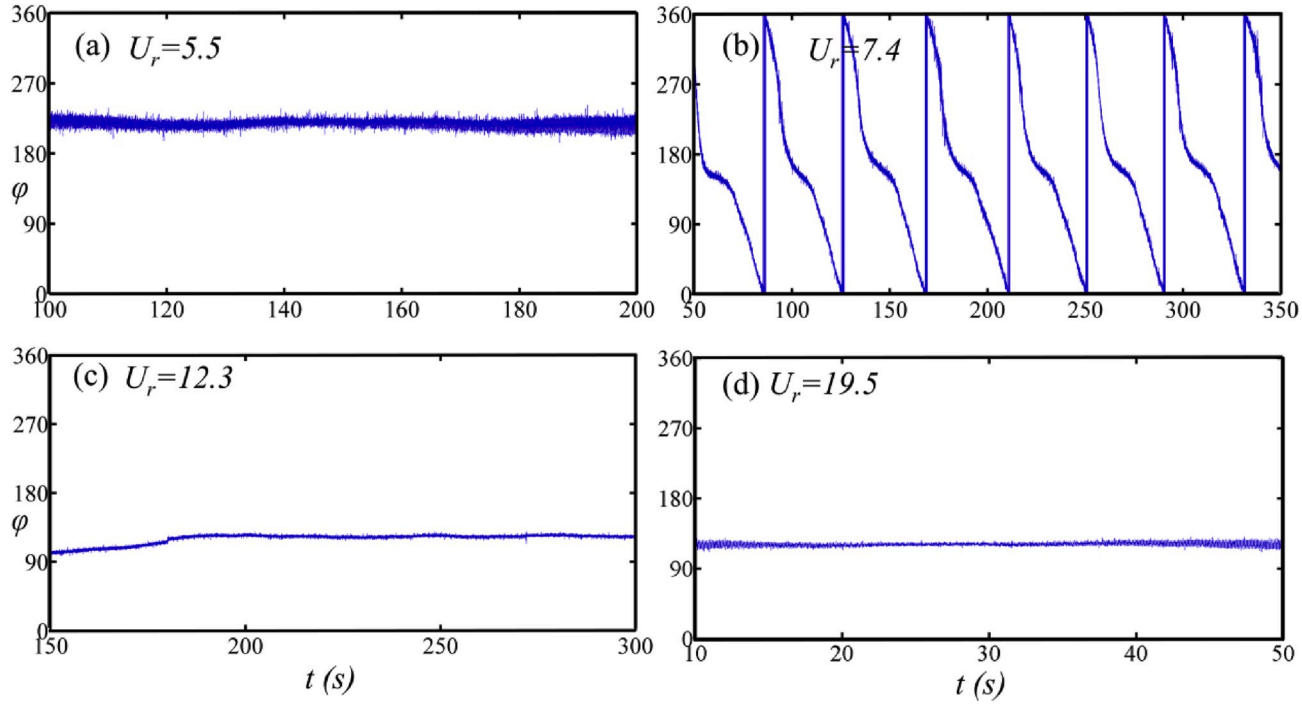

Fig. 9. Phase angle between the displacement responses of the two cylinders versus time at $S/D = 1.2$ for $U_r = 5.5$, 7.4, 12.3, 19.5.

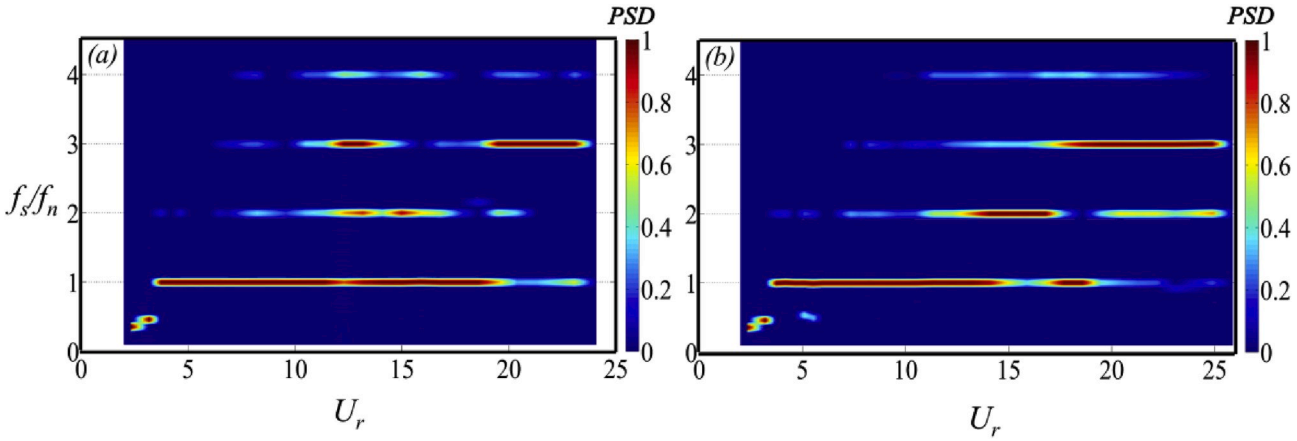

Fig. 10. Normalized *PSD* of vortex shedding frequency for downstream cylinder at (a) $S/D = 1.2$, and (b) 1.5.

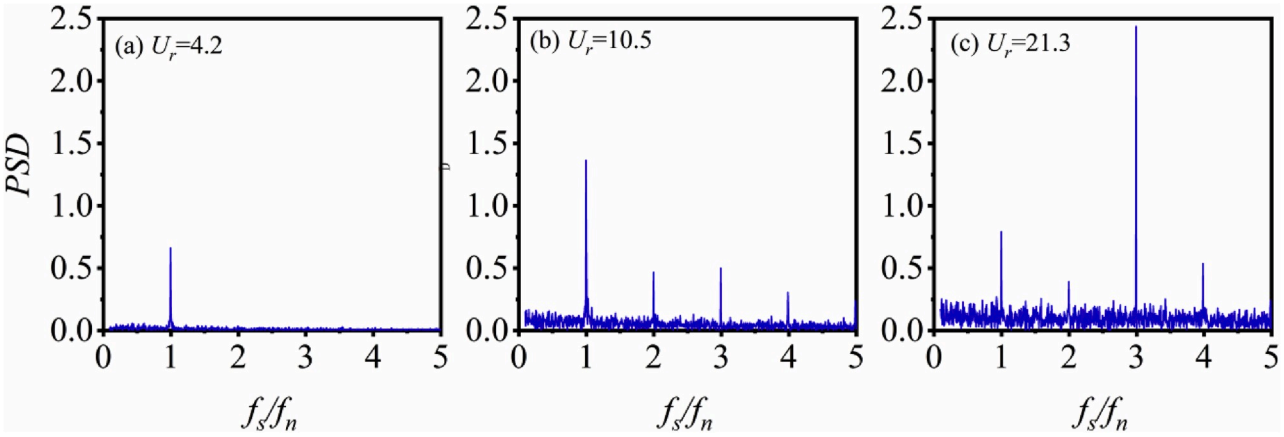

Fig. 11. Normalized *PSD* of vortex shedding frequency of (a) $U_r = 4.2$, (b) 10.5, and (c) 21.3 at $S/D = 1.2$.

VIV response with a broader range of $4.6 \leq U_r \leq 12.3$ than that of the single cylinder ($4.6 \leq U_r \leq 8.7$) and then remains zero until $U_r = 14.1$. For $U_r > 14.1$, it starts to vibrate again and maintains nearly a stable state with the maximum $A_u^n \approx 0.28$. VIV also occurs for the downstream cylinder at $4.6 \leq U_r \leq 12.3$ and A_d^nsharply increases to a very large amplitude oscillation with the maximum $A_d^n \approx 1.03$ after the same onset of vibration of upstream cylinder. It can be observed in Fig. 5 d ($S/D = 3.0$), the VIV regions of upstream and downstream cylinders narrow down to $4.6 < U_r < 9.6$ and almost consistent with the single cylinder. At $U_r > 11.4$, the upstream cylinder presents a very weak vibration though A_d^n still rises, while the rear one gradually increases and experiences a violent vibration, we also called wake-induced galloping (WIG) vibration. The WIG is first pointed out by Bokaian et al. (1984a) which has been introduced at the beginning. It is different from the galloping vibration of the upstream cylinder at $S/D = 1.2$ and 1.5, though both present a violent vibration. That is because the incoming flow past the upstream cylinder is uniform, while the downstream cylinder will be affected by the wake of the front one rather than the uniform incoming

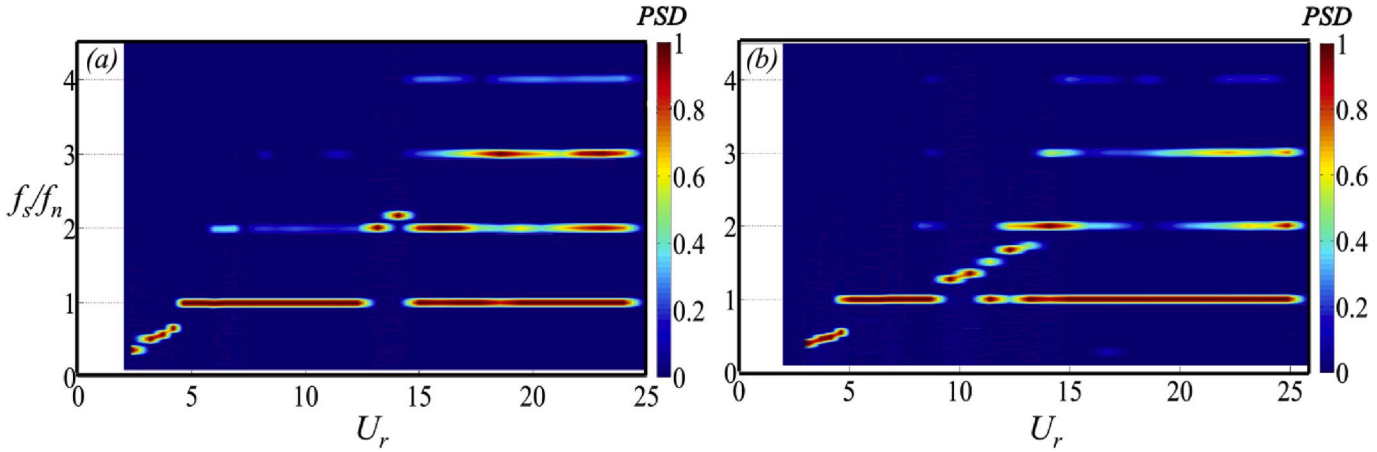

Fig. 12. Normalized *PSD* of vortex shedding frequency for downstream cylinder (a) at $S/D = 2.0$, and (b) $S/D = 3.0$.

flow. Therefore, the WIG can be attributed to the unsteady vortex-structure interactions between the downstream cylinder and the vortex shedding from the upstream one, whereas the galloping vibration for the upstream cylinder can be ascribed to the existence of a fixed downstream cylinder which will be discussed later. It is worth noting that WIG is also called other terminologies in the published literature, such as 'interference galloping' (Ruscheweyh et al., 1992), 'wake galloping' (Brika et al., 1999), 'wake-induced vibration (WIV)' (Assi et al., 2010) or just 'galloping' (Qin et al., 2017).

Fig. 12 a and b depict f_s/f_n as a function of U_r for downstream cylinder at $S/D = 2.0$ and 3.0, respectively. Similarly, two separated regions can also be identified from Fig. 12 a and b. In the first region, the vortex shedding frequency f_s is locked to the first harmonic of f_n, whereas in the second region it is locked to multiple harmonics of f_n. Between the two regions, it follows a linear branch like a stationary cylinder implying the absence of vibration. At $S/D = 2.0$ (Fig. 12 a), for $U_r < 4.6$ and $12.3 < U_r < 14.1$, f_s/f_n with $St \approx 0.15$ and 0.18 can be detected respectively because of the weak or no vibration, VIV appears over a broader range of $4.6 \leq U_r \leq 12.3$ with $f_s = f_n$. The violent vibration occurs for $U_r \geq 14.1$ with $f_s = f_n$, $2f_n$ and $3f_n$. The characteristic of vortex shedding frequency at $S/D = 3.0$ (Fig. 12 b) is similar to that of $S/D = 2.0$ except a narrow lock-in region ($4.6 < U_r < 9.6$) and a slight broader linear branch ($9.6 \leq U_r \leq 12.4$). This can be attributed to that the downstream cylinder sharply increases to a very large amplitude oscillation at $S/D = 2.0$, nevertheless for $S/D = 3.0$, it gradually increases and the upstream cylinder presents weak vibration in the region of $9.6 \leq U_r \leq 12.4$ (see in Fig. 5 c and d).

4.1.3. Vibration characteristics in Regime III ($3.0 < S/D \leq 8.0$)

In Regime III, the upstream cylinder presents a typical VIV with a limited resonance range just like a single cylinder, which implies the downstream cylinder has no more influence on the front one. While the downstream cylinder displays two regions including a VIV and a WIG region, the two regions can be separated or combined. As can be observed from Fig. 5 e, f and g, A_d^n in the WIG region gradually decreases since the diminishing influence of upstream cylinder. For example, it decreases from 1.13D ($S/D = 4.0$) to 0.45D ($S/D = 8.0$). In fact, it can be inferred that the downstream cylinder will be identical to a single cylinder beyond a critical large spacing ratio S/D as well. It is worthwhile mentioned that theA_d^n exhibits two peaks in the VIV region (see in Fig. 5 e for $4.2 \leq U_r \leq 9.7$), this can be ascribed to the influence of the vibrating state of upstream cylinder (strong or weak) which will be systematically discussed in section 4.4.

Fig. 13 a, b and c plot the vortex shedding frequency ratios f_s/f_n for downstream cylinder at $S/D = 4.0$, 6.0 and 8.0, respectively. At $S/D = 4.0$ (Fig. 13 a), the value of f_s/f_n equals 1.0 for $4.6 \leq U_r \leq 9.7$, indicating the occurrence of VIV. For $U_r > 12.1$, the WIG of downstream cylinder takes place along with f_s locked to multiple harmonics of f_n. It follows a linear branch between the two regions of U_r. This is consistent with the amplitude response (a separated VIV and WIG) shown in Fig. 5 e. However, as shown in Fig. 13 b ($S/D = 6.0$), two distinct branches can be detected. In the first branch (the low branch), the vortex shedding frequency f_s remains equal to the natural frequency f_n associating with a whole lock-in region from 5.1 to the maximum U_r in this experiment. Therefore, in Fig. 5 f, the VIV region is combined with the WIG region instead of separating at $S/D = 4.0$ and 8.0. While the other branch (the high branch) is distinctly following $St = 0.18$ line, which may correspond to the vortex shedding frequency from upstream cylinder, or downstream cylinder, or both, as pointed out by Assi et al. (2010). Note that, for $U_r > 12.3$, the first branch has higher energy than the second branch, implying the wake from the upstream cylinder is weak. At $S/D = 8.0$ (Fig. 13 c), two branches can also be evidently observed. Comparing with the graph at $S/D = 6.0$, the first branch ($f_s/f_n = 1$) is broken at $11.4 < U_r < 15.9$ for the absence of vibration leading to a separated VIV and WIG in amplitude response (see in Fig. 5 g).

The vortex shedding frequencies for upstream cylinder at $S/D = 4.0$, 6.0 and 8.0 are shown in Fig. 14. It is clear that the non-dimensional frequencies f_s/f_n of the upstream cylinder at $S/D = 4.0$, 6.0, 8.0 have the similar characteristic to the single elastically mounted cylinder. There exists a lock-in region with $f_s/f_n = 1$ and beyond the region they almost follow $St \approx 0.18$–0.19 line. This also can be revealed in Fig. 5 e, f and g that the upstream cylinder presents a typical VIV with a limited

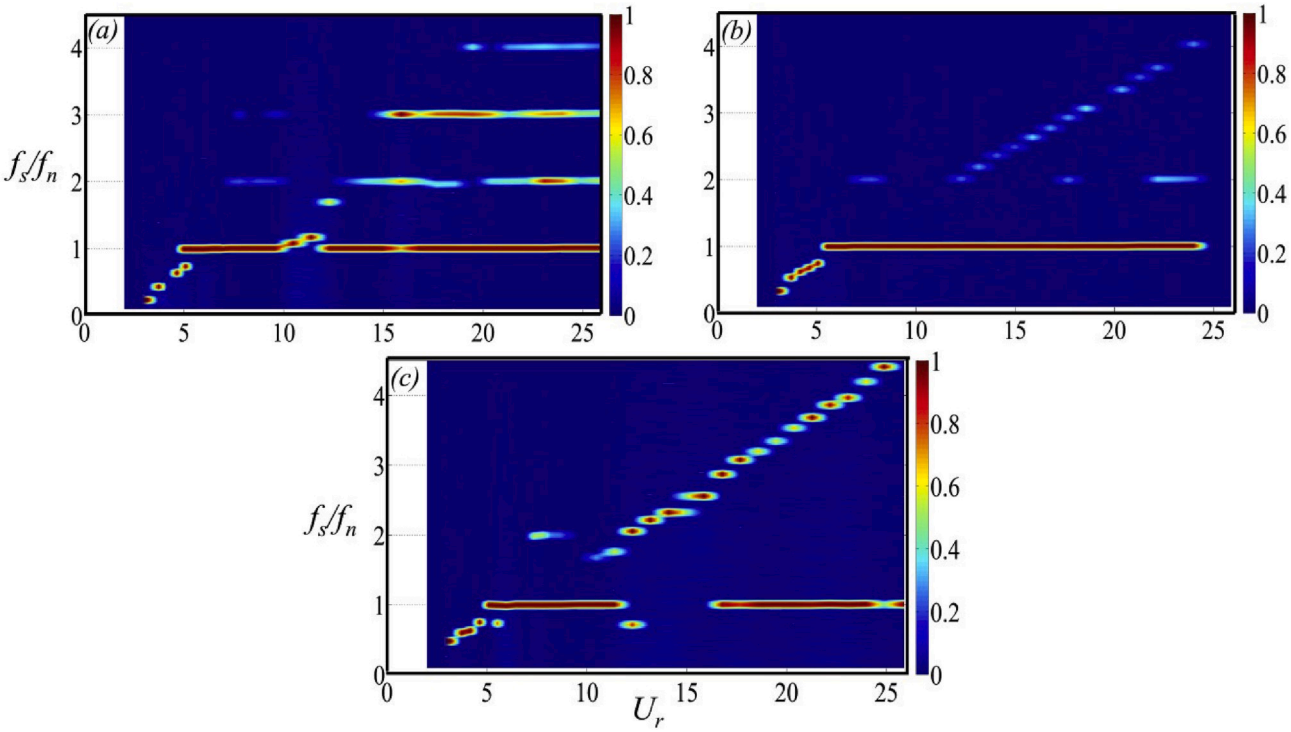

Fig. 13. Normalized *PSD* of vortex shedding frequency for downstream cylinder at (a) $S/D = 4.0$, (b) $S/D = 6.0$ and (c) $S/D = 8.0$.

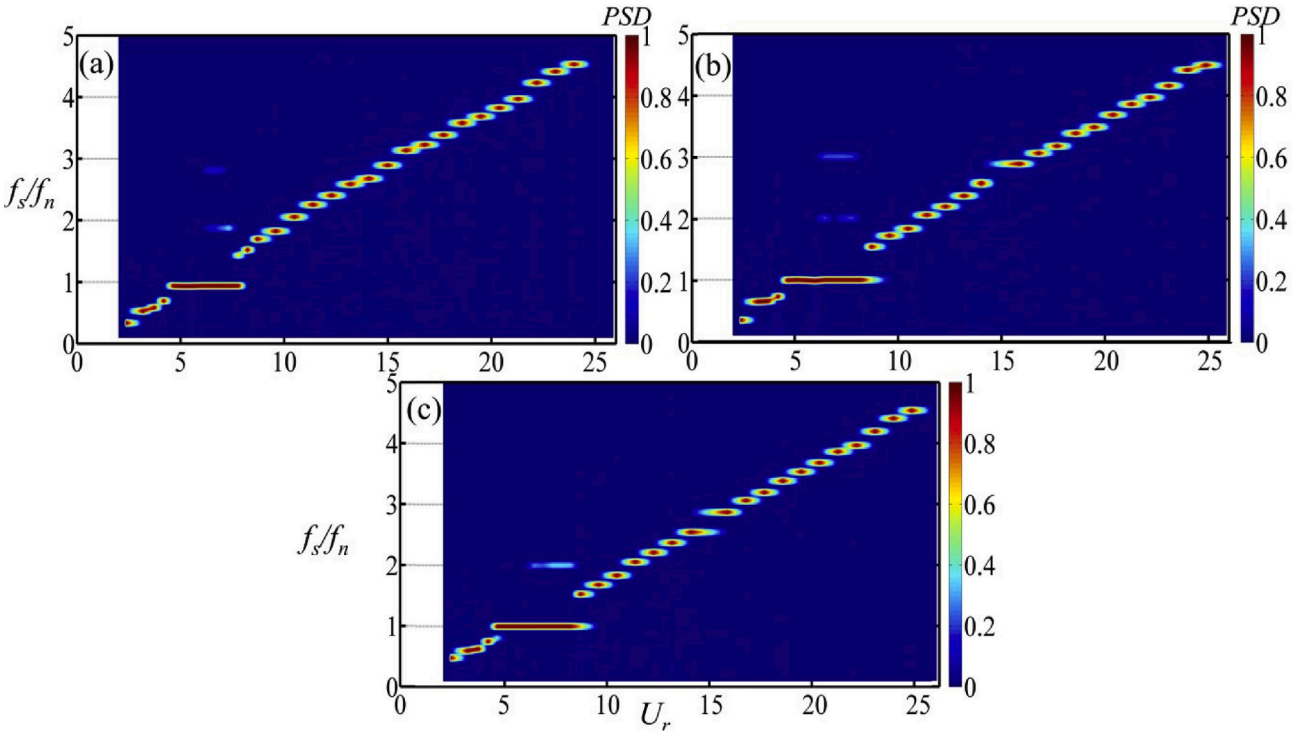

Fig. 14. Normalized *PSD* of vortex shedding frequency for upstream cylinder at (a) $S/D = 4.0$, (b) $S/D = 6.0$ and (c) $S/D = 8.0$.

resonance range.

4.1.4. The discussion of reliability and reproducibility of the results

The occurrence of error is inevitable for an experimental study, therefore it is necessary to discuss the reliability and reproducibility of the results. Fig. 15 presents the test results (A/D) of two times (named test 1 and test 2) along with error bars for each test. The representative spacing ratios $S/D = 1.2$, 3.0 and 8.0 are chosen for brevity. The bars represent the standard deviations achieved by the test data for each reduced velocity U_r. Larger bars mean that the greater deviation of A/D from cycle to cycle.

It can be observed from Fig. 15 that the standard deviations are relatively small especially when the vibration is very weak and the maximum value of the standard deviations occur at $U_r = 7.4$ for $S/D = 1.2$ when the cylinder suffer beating phenomenon (see in Fig. 7 d). This indicates that the vibrations are fairly regular and stable besides the occurrence of beating vibration. The test results of two times are roughly the same except for only a few U_r. Therefore, present results have a good reliability and reproducibility and the value of A/D can represent the actual vibrations of the cylinders.

4.2. The response of oscillation frequency

Fig. 16 shows the variation of dominant oscillation frequency ratios f_o/f_n depending on S/D and U_r consisting of the results from Xu et al. (2019) for the upstream and downstream cylinders performed in the water tunnel. For the present investigations using wind tunnel experiment, unlike the characteristics of vortex shedding frequencies f_s locked to the multiple harmonics of natural frequency f_n, it is evident that the dominant data collapse over $f_o/f_n = 1$ line independent of S/D and U_r. This indicates the dominant oscillation frequencies can only be locked to the natural frequency f_n in the whole time once the cylinders begin to vibrate under the experimental conditions in this paper. More insights into the response of dominant oscillation frequency can be obtained by visiting Fig. 17. As shown in Fig. 17, the representative spacing ratios, $S/D = 1.2$ and 1.5, are chosen to show the variation of *PSD* of f_o/f_n as a function of reduced velocity U_r. Results show that the *PSD* value of f_o/f_n maintains one in the whole examined region which is in consistent with that presented in Fig. 16. While, for the experimental results of Xu et al. (2019), the dominant oscillation frequencies f_o for all four spacing ratios ($S/D = 1.57$, 2.57, 3.57 and 4.57) stay above the natural frequency and roughly lower than the $St = 0.2$ line.

The difference response can be ascribed to the mass ratio m^*. As investigated by Govardhan et al. (2000) for the single cylinder, the f_o/f_n follows $St = 0.17$ line with $m^* = 0.52$, but f_o will be locked to f_n when $m^* = 10.3$, suggesting that the mass ratio m^* plays a significant influence on the response of oscillation frequency. The m^* in present study is 268.9 ($m = 341.9$g, $m_a = 1.27$g) and that in Xu et al. (2019) is 1.34 ($m = 7286$g, $m_a = 5245$g), where the m_a is the value of added mass in still fluid. It is evident that the actual mass of the cylinder is about three hundred times bigger than the added mass m_a at present study in air. However, they are relatively close in Xu et al. (2019) in water. The large m^* are evidently less affected by m_a, therefore the f_o will roughly not change during the vibration with $f_o/f_n = 1$ in wind tunnel experiment. However, for small m^* in water, the added mass m_a may have a pronounced impact on the f_o. As a result, the response of oscillation frequency f_o in water will be changed and it is not always equal to f_n.

4.3. Influence of different test initial conditions ('from rest' and 'increasing velocity')

Two test initial conditions, 'from rest' and 'increasing velocity', are performed in the experiment for the two cylinders. The procedure of 'from rest' can be illustrated as following: for each test, the speed of incoming flow is started from 0 and at this time the cylinder is in the state of rest. Afterwards, accelerate the speed up to the targeted value, maintain the speed until the cylinder achieve a stable periodic vibration. And then stop the wind tunnel motor when finish the test. It can be obtained different reduced velocity by running the test at different velocities. While, the 'increasing velocity' is to make the cylinders start to vibrate at the steady-state amplitude produced by the previous U_r and then continuously increasing to a new targeted U_r without outside

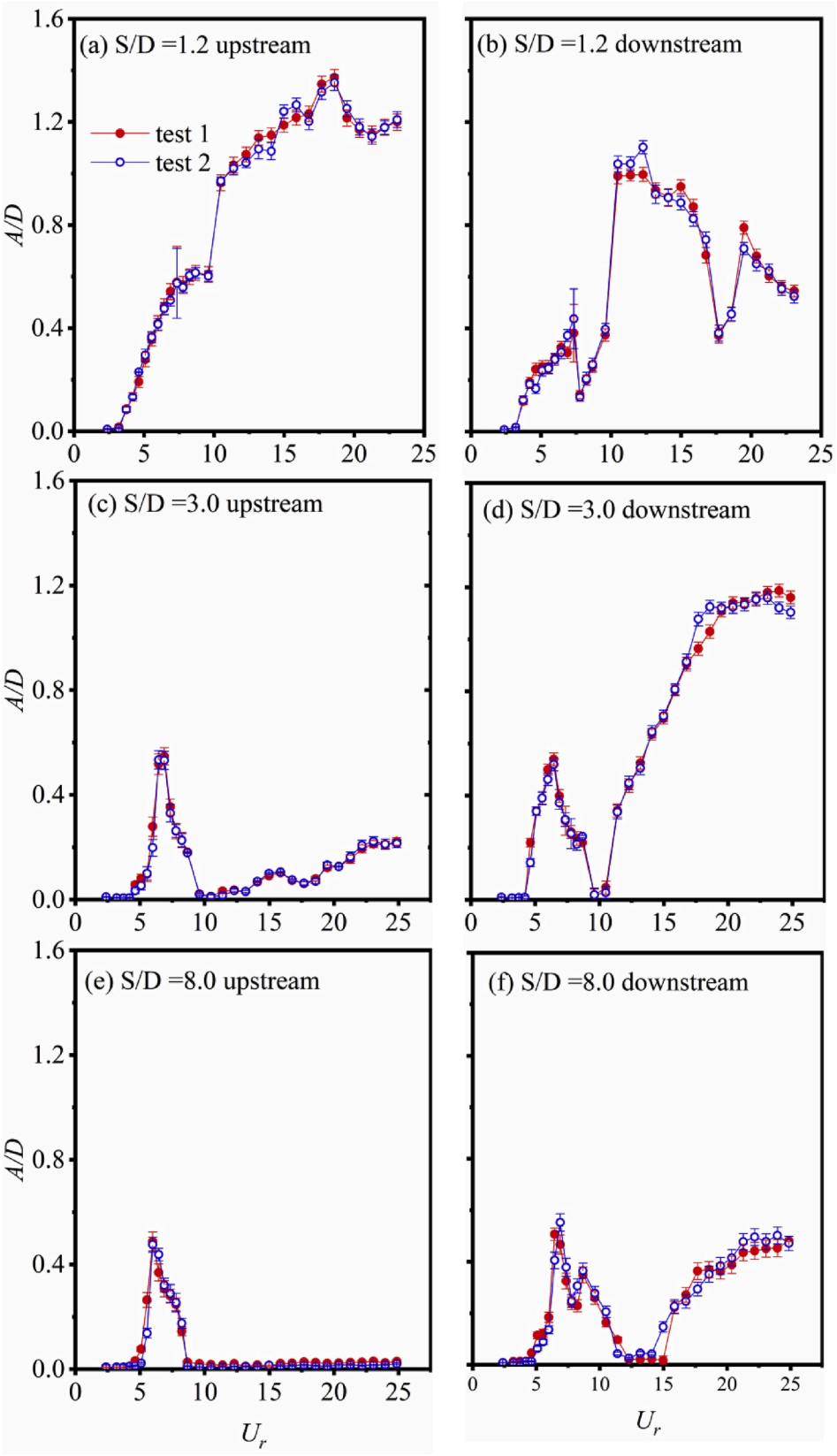

Fig. 15. Test A/D of two times along with standard deviations varying with U_r for upstream and downstream cylinders at different S/D (a) and (b) $S/D = 1.2$, (c) and (d) 3.0, (e) and (f) 8.0.

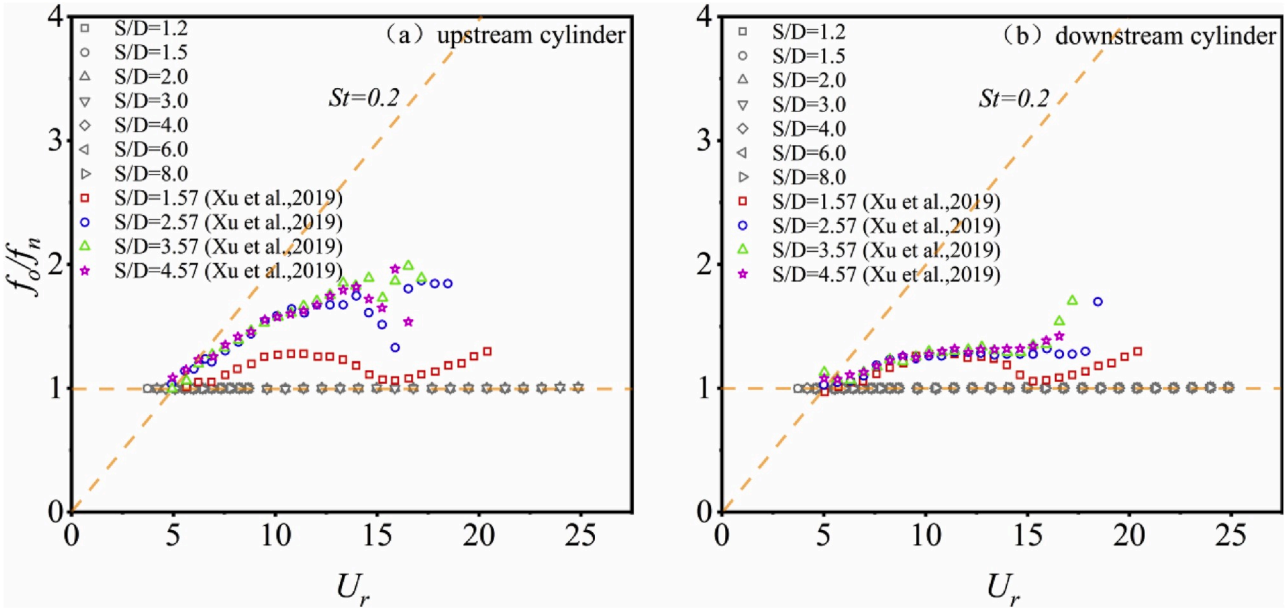

Fig. 16. Variation of dominant oscillation frequencies depended on S/D and U_r (a) upstream cylinder, and (b) downstream cylinder.

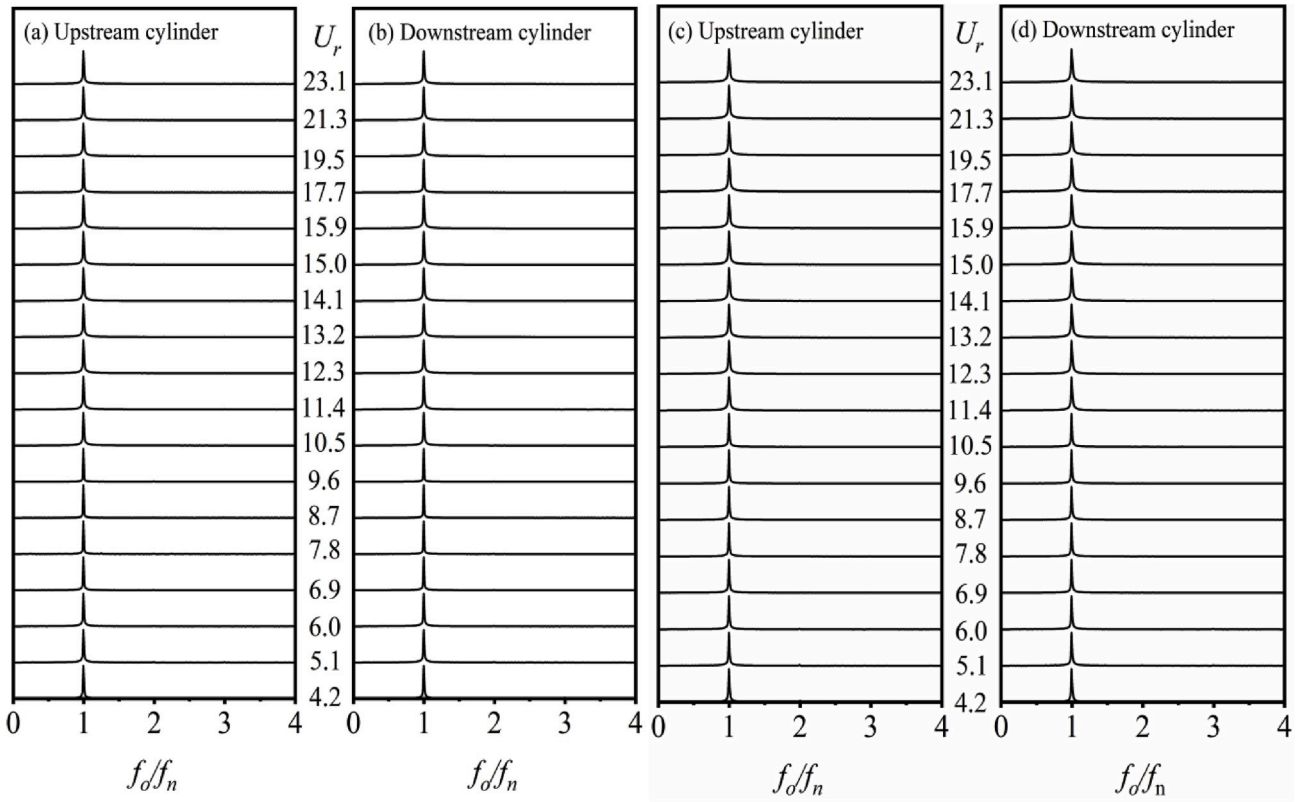

Fig. 17. *PSD* of oscillation frequencies (a) and (b) at $S/D = 1.2$; (c) and (d) at $S/D = 1.5$.

interference.

In order to have a better understanding of the procedure of different initial conditions, a sample of time histories of 'from rest' and 'increasing velocity' at the same objective $U_r = 14.1$ at $S/D = 4.0$ are shown in Fig. 18. As can be seen from Fig. 18, the amplitude of cylinder is from 0 to a final stable periodic vibration for the case of 'from rest'. While, for 'increasing velocity', the cylinder starts to vibrate with an initial steady-state amplitude produced by the previous $U_r = 12.3$, and then increases to a final stable periodic vibration.

How do the 'from rest' and 'increasing velocity' affect the vibration response? The work in this section aims to address the above issue.

According to the S/D that the three classified regimes at, the compare of vibration responses for 'from rest' and 'increasing velocity' are shown in Figs. 19–21, respectively. As observed from the graphs, two vibration features can be identified. At $S/D = 1.2$, 3.0, 4.0, 6.0, 8.0, the vibration trends of 'from rest' are nearly the same to the case of 'increasing velocity' for the both cylinders, there exist no hysteresis phenomenon. While, at $S/D = 1.5$ and 2.0, two obviously different vibration trends and

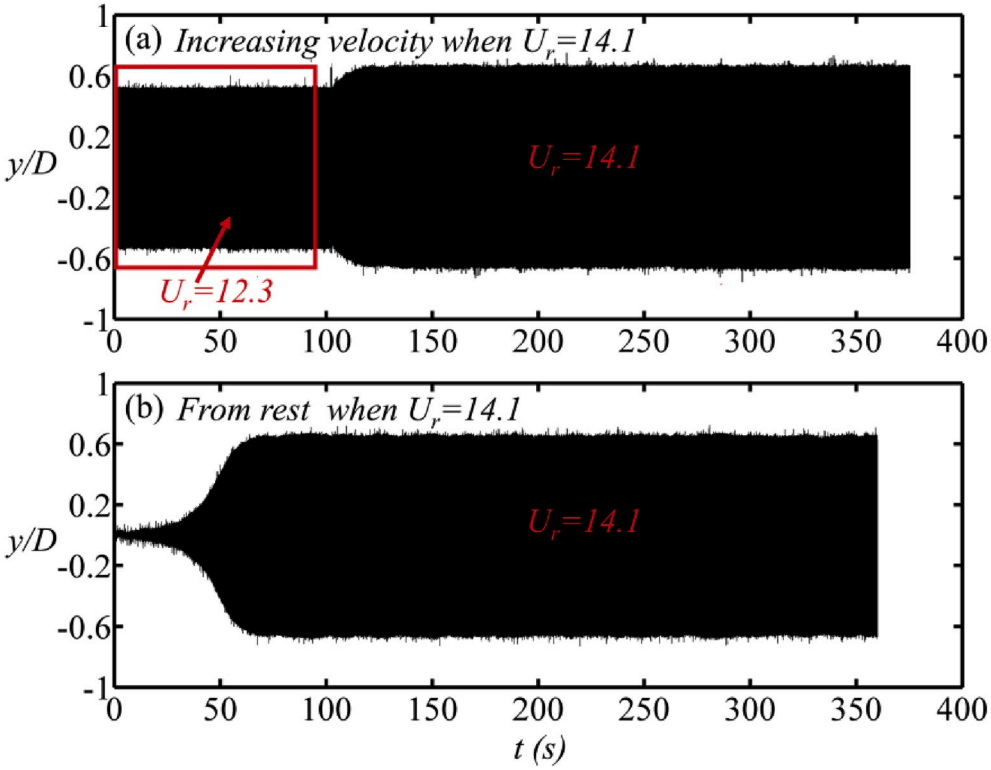

Fig. 18. Sample of time histories of 'from rest' and 'increasing velocity' at same objective $U_r = 14.1$ at $S/D = 4.0$.

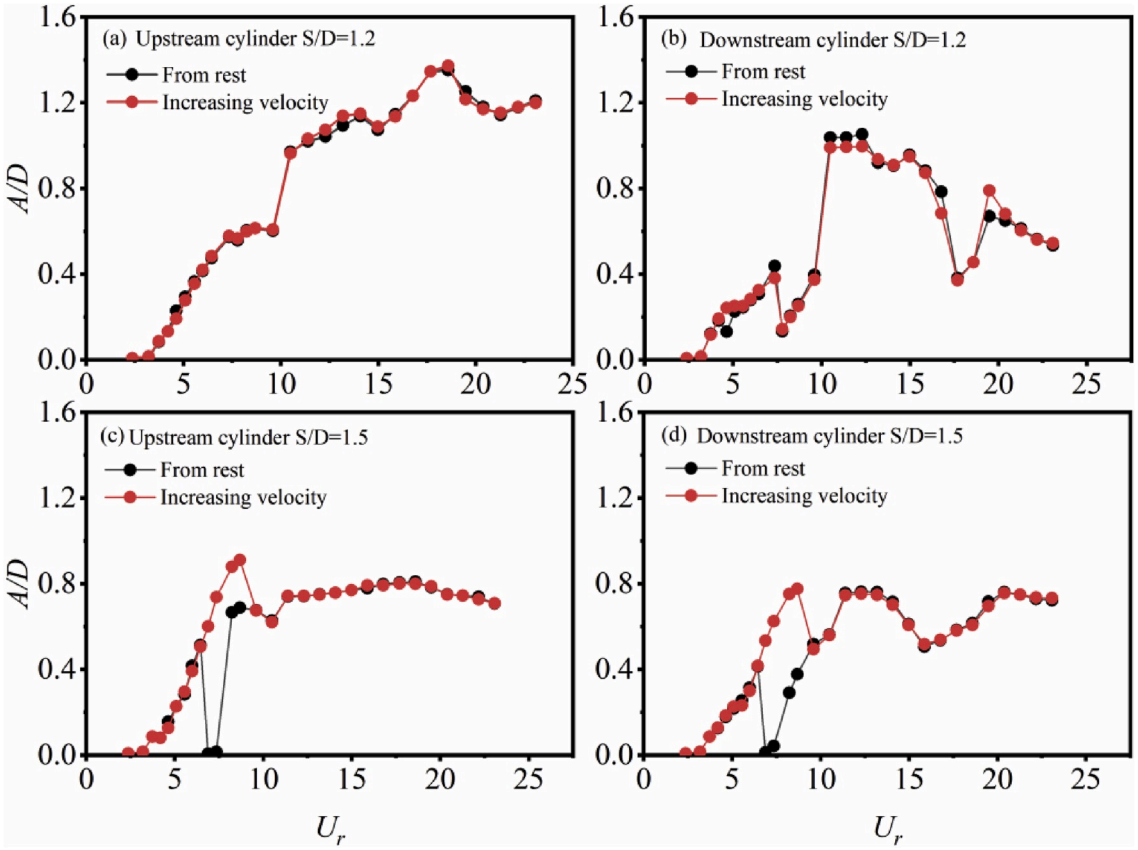

Fig. 19. Amplitude response versus U_r for 'increasing velocity' and 'from rest' depended on S/D and U_r. (a) and (c) Upstream cylinder at $S/D = 1.2, 1.5$; (b) and (d) Downstream cylinder at $S/D = 1.2, 1.5$.

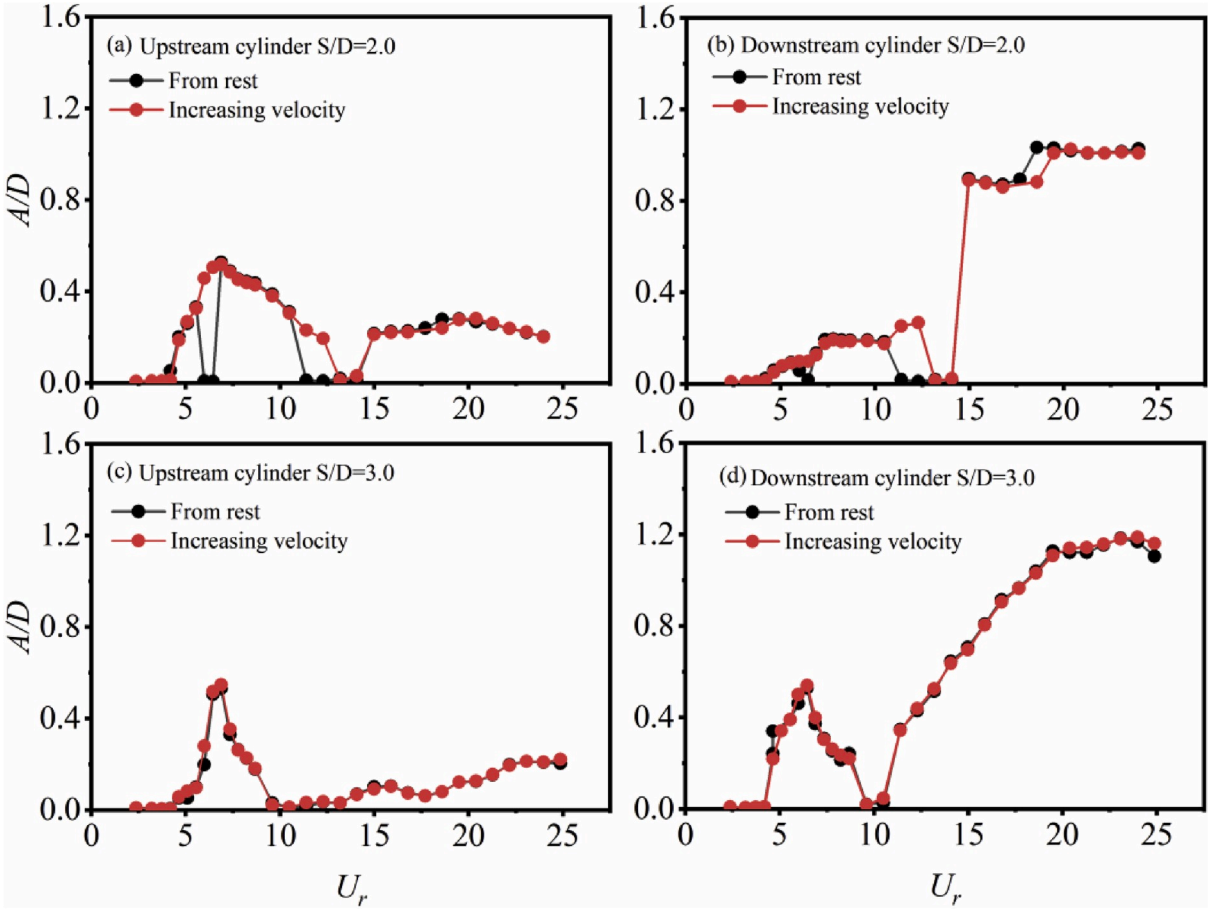

Fig. 20. Amplitude response versus U_r for 'increasing velocity' and 'from rest' depended on S/D and U_r. (a) and (c) Upstream cylinder at $S/D = 2.0$, 3.0; (b) and (d) Downstream cylinder at $S/D = 2.0$, 3.0.

a hysteresis phenomenon for 'from rest' and 'increasing velocity' can be observed as a function of U_r.

For the upstream cylinders at $S/D = 1.5$ (Fig. 19 c), both of them start to vibrate at $U_r = 3.7$ and A_u^n nearly follow the same trend until at $U_r = 6.4$, which approaches the point of the maximum amplitude for single cylinder. After this ($U_r > 6.4$), for the case of 'increasing velocity', A_u^n continues to increase rapidly and undergoes a hump with a local peak of 0.91 at $U_r = 8.7$, and then gradually increases again after $U_r = 10.5$, maintaining a large convergent amplitude oscillation with maximum $A_u^n = 0.80$. However, for the case of 'from rest', the absence of vibration takes place in the region of $6.4 \leq U_r \leq 7.3$ and then A_u^n sharply increases to 0.67 at $U_r = 8.2$ which is smaller than that of 'increasing velocity' ($A_u^n = 0.88$). For $U_r \geq 9.6$, the A_u^n of 'from rest' converges to that of 'increasing velocity' again. In Fig. 19 d ($S/D = 1.5$), within the region of $6.4 < U_r < 9.6$, the downstream cylinders also suffer a hysteresis phenomenon which is characterized with two apparent branches under the two initial test conditions. Whereas, beyond the region, A_d^n of 'from rest' keeps the same to that of 'increasing velocity'.

The hysteresis phenomenon presented above can be attributed to the gap flow pointed out by Zdravkovich (1974, 1988), which is triggered by an initial displacement when two cylinders are proximal. Therefore, for instance, the upstream and downstream cylinders can not be excited to vibrate for the condition of 'from rest' due to the stationary state at $6.4 \leq U_r \leq 7.3$. While, the 'increasing velocity' signifies an initial displacement together with a strong gap flow which will produce a large lift force to excite vibration. This is good agreement with the investigations from Zdravkovich (1974) and Hu et al. (2019).

Fig. 20 a and b show the effect of different initial test conditions on the amplitude response of the two cylinders at $S/D = 2.0$. The regions of the occurrence of hysteresis phenomenon for upstream and downstream cylinders become smaller, implying the diminished effect of gap flow between the two cylinders. If further increase S/D ($\geq$3.0), there will be no more hysteretic in the vibration amplitude response since the spacing ratio is large enough and the gap flow disappears gradually (see in Fig. 21). It is interesting that there also exists no hysteresis phenomenon at $S/D = 1.2$ (see in Fig. 19 a and b), though the spacing ratio is smaller than 1.5 and 2.0. The underlying mechanism will be explained and discussed in section 4.4.

To illustrate the characteristics of vibration amplitude response further, the non-dimensional vortex shedding frequency f_s/f_n for 'from rest' at $S/D = 1.5$ (the occurrence of hysteresis phenomenon) and 3.0 (no hysteresis phenomenon) are chosen to present for brevity. Fig. 22 depicts f_s/f_n for the case of 'from rest' as a function of U_r at $S/D = 1.5$. Similar to the different amplitude vibration patterns shown in Fig. 19 c and d, the curves of f_s/f_n for the two initial test conditions exhibit distinctively various trends in the region of $6.4 \leq U_r \leq 7.3$ as well, when the hysteresis phenomenon happens. In comparison with the result of 'increasing velocity' (see in Fig. 10 b), the value of f_s/f_n for 'from rest' follows a linear branch like a stationary cylinder consistent with the absence of vibration at $6.4 \leq U_r \leq 7.3$. At $S/D = 3.0$, by comparing Figs. 12 b and Fig. 23, the graph of f_s/f_n for 'increasing velocity' is same to that of 'from rest', indicating the vortex shedding modes have no difference between them. Therefore, there exist no hysteresis phenomenon and the vibration amplitude responses are nearly identical.

In summary, different vibration amplitude responses can be observed at $S/D = 1.5$ and 2.0 for the two initial test conditions, 'from rest' and 'increasing velocity', used in the current experiment, which is indicative of a hysteresis phenomenon. That is, at some given U_r or Re, the

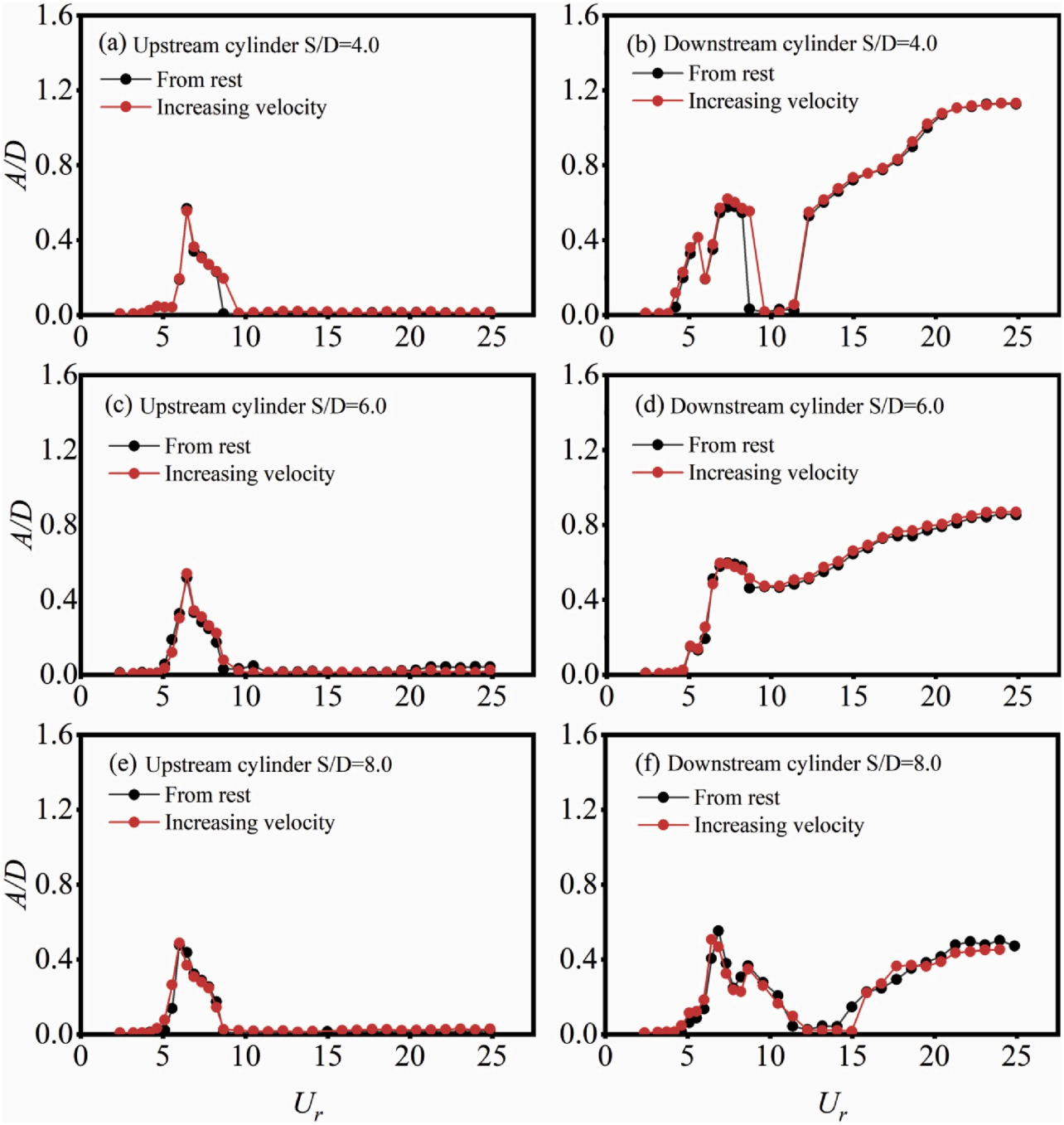

Fig. 21. Amplitude response versus U_r for 'increasing velocity' and 'from rest' depended on S/D and U_r. (a), (c) and (e) Upstream cylinder at S/D = 4.0, 6.0, 8.0; (b), (d) and (f) Downstream cylinder at S/D = 4.0, 6.0, 8.0.

vibrations of cylinders are depended on whether they are vibrating or stationary. On the other hand, with the increasing of S/D ($\geq$3.0), the difference of vibration trend can be negligible, which can be attributed to the gradually decreasing influence of gap flow. As a result, the occurrence of hysteresis is depended on the initial conditions and spacing ratio S/D.

4.4. Influence of initial state (fixed or elastically mounted) of the neighbouring cylinder

The initial states (fixed or elastically mounted) of the neighbouring cylinder may be exerted different influence on the vibration amplitude response of the other one. The experiment is carried out by keeping one of the cylinders fixed or elastically mounted, while the other cylinder can vibrate freely. Just as Kim et al. (2009) stated, investigating this issue is very significant from an engineering point of view. Hence, three spacing ratios, S/D = 1.2, 3.0 and 8.0 representing in Regimes I, II, III, are selected to examine the impact of initial states of one cylinder on the other one, respectively. The results are presented in Fig. 24. The left column of the figure (Fig. 24 a, c and e) compares the vibration amplitude response of upstream cylinder when the downstream cylinder is fixed (black quadrate symbol) or elastically mounted (red quadrate symbol). Similarly, the right (Fig. 24 b, d and f) is the vibration data of the downstream cylinder when the upstream cylinder under different initial states, the black circular symbol represents fixed and the red circular symbol is elastically mounted.

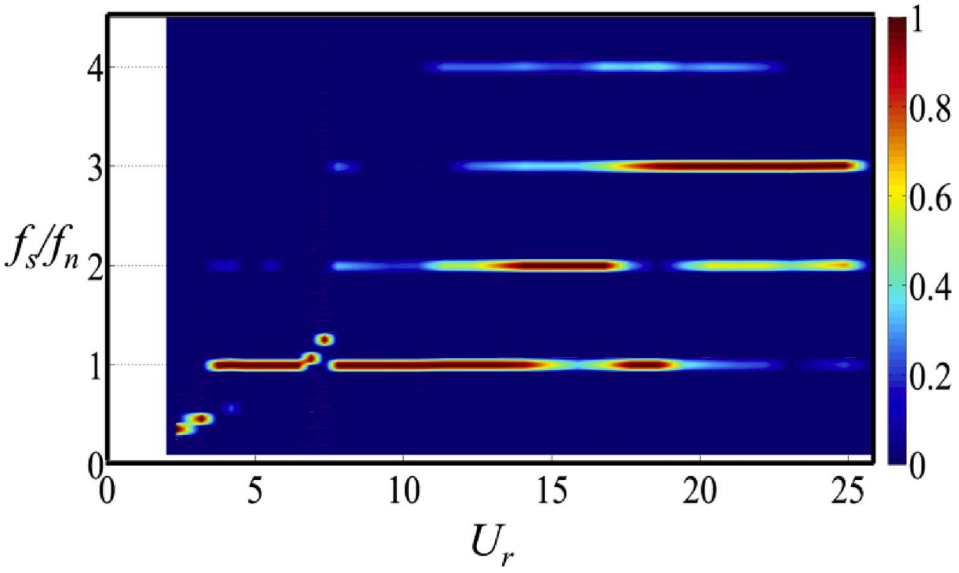

Fig. 22. Normalized *PSD* of vortex shedding frequency at $S/D = 1.5$ for the case of 'from rest'.

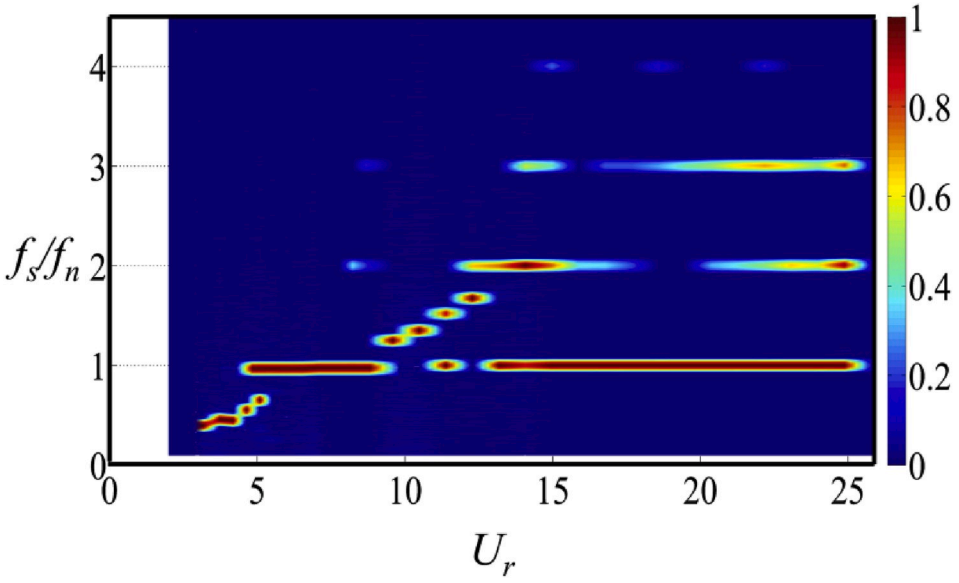

Fig. 23. Normalized *PSD* of vortex shedding frequency at $S/D = 3.0$ for the case of 'from rest'.

As obviously shown in Fig. 24 a and b ($S/D = 1.2$ in Regime I), the response characteristic of upstream cylinder is qualitatively same when the downstream cylinder from fixed to elastically mounted, other than a variation in amplitude. This suggests that the upstream cylinder undergoes galloping vibration just because the existence of a proximal downstream cylinder and nothing to do with the state of the downstream cylinder. Therefore, the hysteresis phenomenon is absence at $S/D = 1.2$ in Fig. 19 a and b. The galloping vibration was also observed by Bokaian et al. (1984b) for the upstream cylinder with a fixed downstream cylinder by using a water tunnel and they emphasized that the essential factor for the occurrence of galloping was that the rear cylinder is well inside the near wake of the front one. While, unlike the fluctuating of A_d^n as the upstream cylinder is in the state of elastically mounted, the downstream cylinder increases sharply at $U_r = 4.2$ and achieves two stable platforms with the maximum $A_d^n = 0.89$ (the first platform) and 1.29 (the second platform) respectively when the upstream cylinder is fixed. From the above observation, it can be implied that, regardless of fixed or not, the interference influence of the downstream cylinder on the upstream is very weak. While, the initial states of the upstream cylinder play a significant effect on the downstream cylinder vibration response.

In Regime II ($S/D = 3.0$), as the downstream cylinder is fixed, the response of the upstream cylinder is similar to that of a single cylinder with a limited resonance region, whereas A_u^n still increases slowly for U_r >11.4 when the downstream cylinder is not fixed. The observation from Fig. 24 c suggests that the downstream cylinder still has a small impact on the upstream cylinder, so it is able to excite the motion of the upstream cylinder once the downstream can vibrate freely. On the other hand, when the upstream cylinder is fixed (Fig. 24 d), the response of A_d^n is similar to the vibrating upstream cylinder except a variation in the region of the existence of VIV, indicating that the interference of the upstream cylinder on the downstream is very small in this regime.

At $S/D = 8.0$ (in Regime III), the variations of A_u^n can be negligible under the two initial states of downstream cylinder (Fig. 24 e), implying the rear cylinder has no more influence on the upstream cylinder. Based on Fig. 24 f, as the upstream cylinder is fixed, it can be found that the

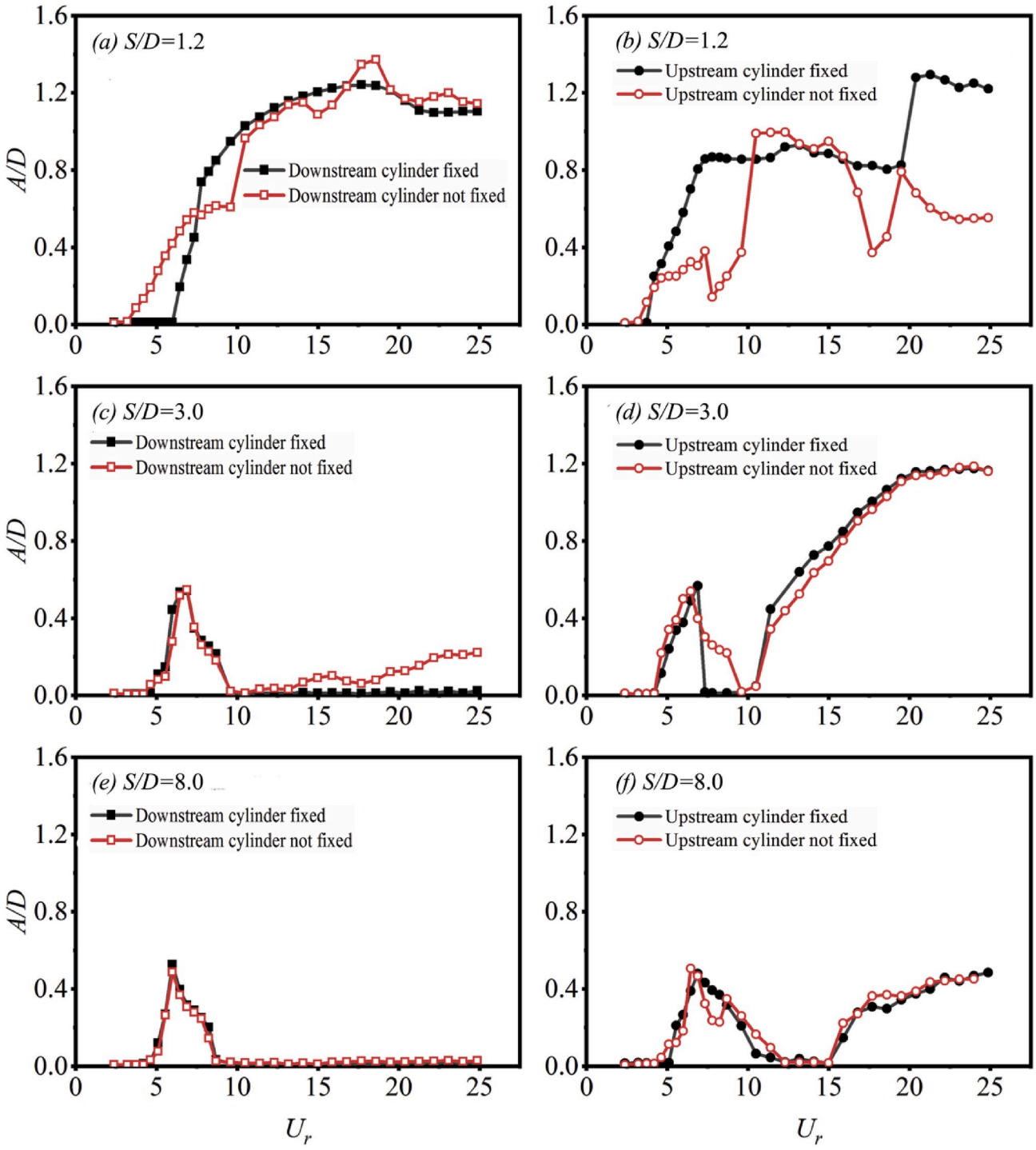

Fig. 24. (a,c,e) Vibration response of the upstream cylinder when downstream cylinder is fixed or elastically mounted; (b,d,f) Vibration response of the downstream cylinder when upstream cylinder is fixed or elastically mounted.

downstream cylinder present two humps with two peaks in the VIV region ($4.6 \leq U_r \leq 12.3$), but outside the region, the A_d^n differs very slightly from the vibrating upstream cylinder. The same phenomenon (two humps) can be also observed at $S/D = 4.0$, 6.0 in Regime III (Fig. 5 e and f). This can be attributed to the sudden change of vortex shedding frequency f_s when the upstream cylinder from stationary to vibration. For the case of stationary upstream cylinder, the f_s ($= USt/D$) depends on the incoming velocity U, where St is the strouhal number with the value of 0.2; On the other hand, once the upstream cylinder is able to vibrate (in the lock-in region), the f_s will be locked to the natural frequency of the upstream cylinder along with 2S or 2P mode (according to the value of reduced velocity U_r) and do not vary with the incoming velocity U. Therefore, that is why the inflection point between the two humps occurs at the onset or end of vibration of upstream cylinder.

From what has been discussed above, it is worthwhile mentioned that the effect of the initial states of the neighbouring cylinder on the other cylinder is different from one regime to another for Regimes I, II and III with the increasing of spacing ratio S/D.

5. Conclusions

The cross-flow vibrations of two identical elastically mounted cylinders in tandem arrangement are experimentally investigated using a low turbulence wind tunnel. The parameters contain spacing ratio S/D ($= 1.2$–8.0), reduced velocity U_r ($= 2.4$–25.0) and Reynolds number Re ($=$ 4000–42000). Results are presented in the form of amplitude response, oscillation frequency f_o and vortex shedding frequency f_s. The research covers four aspects, i.e. a preliminary test for the single cylinder, the particularly studied on the vibration characteristics of the two cylinders depend on S/D and U_r for 'increasing velocity', the influence of initial test conditions ('from rest' and 'increasing velocity') on the vibration responses of the two cylinders, the influence of initial states (fixed or elastically mounted) of the neighbouring cylinder on the other one. Based on the presented results and discussions, several conclusions can be summarized as following.

Depended on the characteristics of vibration, three regimes can be classified. In Regime I ($S/D \leq 1.5$), the upstream cylinder experiences galloping vibration, while the amplitude of downstream cylinder (A_d^n) undergoes fluctuating with multiple peaks versus U_r, and the amplitude of upstream cylinder (A_u^n) is roughly greater thanA_d^n; In Regime II ($1.5 <$ S/D ≤ 3.0), it is characterized by two separated vibration regions for both upstream and downstream cylinders. In the first region, A_u^n is greater thanA_d^n, while in the second region, A_u^n is smaller thanA_d^n. In Regime III ($3.0 <$ S/D ≤ 8.0), the upstream cylinder presents a typical VIV just like a single cylinder, while the downstream cylinder displays two regions including a VIV and a WIG region, the two regions can be separated or combined. For the influence of 'from rest' and 'increasing velocity', an obvious hysteresis phenomenon of vibration responses can be observed at $S/D = 1.5$ and 2.0. While, at $S/D \geq 3.0$, the hysteresis phenomenon can be negligible. The effect of the initial states of the neighbouring cylinder on the other cylinder is different from one regime to another. For instance, in Regimes I, the initial states of the upstream cylinder play a pronounced effect on the downstream cylinder, while the influence of the downstream cylinder exerts on the upstream is very weak. In Regime II, the initial states of the downstream cylinder have small influence on the front one and the upstream cylinder show weak effect on the rear one as well.

The f_s is also influenced by S/D and U_r. In Regimes I, f_s can be locked to multiple harmonics of natural frequency f_n during the galloping vibration and the dominant value of f_s/f_n changes with the increasing of U_r. In Regimes II, two separated regions can be identified consistent with the amplitude responses. In the first region, f_s is locked to the first harmonic of f_n, whereas in the second region it is locked to multiple harmonics of f_n. In Regimes III, two distinct branches can be detected. In the first branch, f_s remains equal to f_n, while the other branch is distinctly following $St = 0.18$ line. Unlike the characteristics of f_s, the features of f_o are obviously different between low mass ratio and high mass ratio. The dominant f_o can only be locked to the f_n in the whole time once the cylinders begin to vibrate for high mass ratio, while it will stay above the f_n and roughly lower than $St = 0.2$ line for low mass ratio.

Declaration of competing interest

The authors declare that they have no known competing financial interests or personal relationships that could have appeared to influence the work reported in this paper.

CRediT authorship contribution statement

Zhongming Hu: Writing - original draft, Visualization, Investigation, Validation, Methodology, Conceptualization. **Jiasong Wang:** Conceptualization, Methodology, Resources, Writing - review & editing, Supervision, Funding acquisition. **Yuankun Sun:** Visualization, Investigation, Methodology.

Acknowledgements

The authors are grateful to the financial support from the National Natural Science Foundation of China (Grant No. 11872250), National Basic Research Program of China (973 Program) (Grant No. 2015CB251203) and National Major Science and Technology Project of China (Grant No. 2016ZX05028-001).

Appendix A. Supplementary data

Supplementary data to this article can be found online at https://doi.org/10.1016/j.oceaneng.2020.107501.

References

Armin, M., Khorasanchi, M., Day, S., 2018. Wake interference of two identical oscillating cylinders in tandem: an experimental study. Ocean. Eng. 166, 311–323.
Assi, G.R.S., Bearman, P.W., Meneghini, J.R., 2010. On the wake-induced vibration of tandem circular cylinders: the vortex interaction excitation mechanism. J. Fluid Mech. 661, 365–401.
Assi, G.R.S., Bearman, P.W., Carmo, B.S., Meneghini, J.R., Sherwin, S.J., Willden, R.H.J., 2013. The role of wake stiffness on the wake-induced vibration of the downstream cylinder of a tandem pair. J. Fluid Mech. 718, 210–245.
Bearman, P.W., 1984. Vortex shedding from oscillating bluff bodies. Annu. Rev. Fluid Mech. 16 (1), 195–222.
Blevins, R.D., 1990. Flow-induced Vibration, second ed. Van Nostrand, Reinhold, New York, USA.
Bokaian, A., Geoola, F., 1984a. Wake-induced galloping of two interfering circular cylinders. J. Fluid Mech. 146, 383–415.
Bokaian, A., Geoola, F., 1984b. Proximity-induced galloping of two interfering circular cylinders. J. Fluid Mech. 146, 417–449.
Borazjani, I., Sotiropoulos, F., 2009. Vortex-induced vibrations of two cylinders in tandem arrangement in the proximity wake interference region. J. Fluid Mech. 621, 321–364.
Brika, D., Laneville, A., 1999. The flow interaction between a stationary cylinder and a downstream flexible cylinder. J. Fluid Struct. 13, 579–606.
Chen, W.L., Ji, C.N., Williams, J., Xu, D., Yang, L.H., Cui, Y.T., 2018. Vortex-induced vibrations of three tandem cylinders in laminar cross-flow: vibration response and galloping mechanism. J. Fluid Struct. 78, 215–238.
Feng, C.C., 1968. The Measurement of Vortex Induced Effects in Flow Past Stationary and Oscillating Circular and D-Section Cylinders. Master's thesis, Department of Mechanical Engineering, The University of British Columbia, Canada.
Govardhan, R., Williamson, C., 2000. Modes of vortex formation and frequency response of a freely vibrating cylinder. J. Fluid Mech. 420, 85–130.
Griffin, O.M., 1980. Vortex-excited cross flow vibrations of a single circular cylinder. ASME J. Press Vessel Technol 102, 158–166.
Gu, F., Wang, J.S., Qiao, X.Q., Huang, Z., 2012. Pressure distribution, fluctuating forces and vortex shedding behavior of circular cylinder with rotatable splitter plates. J. Fluid Struct 28, 263–278.
Hover, F.S., Triantafyllou, M.S., 2001. Galloping response of a cylinder with upstream wake interference. J. Fluid Struct. 15 (3–4), 503–512.
Hu, Z.M., Wang, J.S., Sun, R., Zhou, J.L., Xu, L.B., Sheng, L.X., 2019. Cross-flow vibration response for one-fixed-one-free tandem arrangement cylinders with large mass ratio using wind tunnel experiment. In: The 29th International Ocean and Polar Engineering Conference. International Society of Offshore and Polar Engineers, ISOPE, Honolulu, Hawaii, USA, June 16-21.
Huang, S., Herfjord, K., 2013. Experimental investigation of the forces and motion responses of two interfering VIV circular cylinders at various tandem and staggered positions. Appl. Ocean Res. 43, 264–273.
Huang, S., Sworn, A., 2011. Some observations of two interfering VIV circular cylinders of unequal diameters in tandem. J. Hydrodyn. Ser. B 23 (5), 535–543.
Huera-Huarte, F.J., Bearman, P.W., 2011. Vortex and wake-induced vibrations of a tandem arrangement of two flexible circular cylinders with near wake interference. J. Fluid Struct. 27 (2), 193–211.
Huera-Huarte, F.J., Gharib, M., 2011. Vortex and wake-induced vibrations of a tandem arrangement of two flexible circular cylinders with far wake interference. J. Fluid Struct. 27 (5), 824–828.
Igarashi, T., 1981. Characteristics of the flow around two circular cylinders arranged in tandem. Bull. JSME. 24 (188), 323–331.
Khalak, A., Williamson, C.H.K., 1999. Motions, forces and mode transitions in vortex-induced vibrations at low mass-damping. J. Fluid Struct. 13, 813–851.
Kim, S., Alam, M.M., Sakamoto, H., Zhou, Y., 2009. Flow-induced vibrations of two circular cylinders in tandem arrangement. Part I. Characteristics of vibration. J. Wind Eng. Ind. Aerod. 97, 304–311.
Liang, S.P., Wang, J.S., Hu, Z.M., 2018. VIV and galloping response of a circular cylinder with rigid detached splitter plates. Ocean. Eng. 162, 176–186.
Lin, K., Wang, J.S., Zheng, H.X., Sun, Y.K., 2020. Numerical investigation of flow-induced vibrations of two cylinders in tandem arrangement with full wake interference. Phys. Fluids 32, 015112.
Mittal, S., Kumar, V., 2001. Flow-induced oscillations of two cylinders in tandem and staggered arrangements. J. Fluid Struct. 15 (5), 717–736.

Papaioannou, G.V., Yue, D.K.P., Triantafyllou, M.S., Karniadakis, G.E., 2008. On the effect of spacing on the vortex-induced vibrations of two tandem cylinders. J. Fluid Struct. 24, 833–854.
Parkinson, G.V., 1989. Phenomena and modelling of flow-induced vibrations of bluff bodies. Prog. Aero. Sci. 26, 169–224.
Prasanth, T.K., Mittal, S., 2009. Flow-induced oscillation of two circular cylinders in tandem arrangement at low Re. J. Fluid Struct. 25, 1029–1048.
Qin, B., Alam, M.M., Zhou, Y., 2017. Two tandem cylinders of different diameters in cross-flow: flow-induced vibration. J. Fluid Mech. 829, 621–658.
Qin, B., Alam, M.M., Ji, C.N., Liu, Y., Xu, S.J., 2018. Flow-induced vibrations of two cylinders of different natural frequencies. Ocean. Eng. 155, 189–200.
Ruscheweyh, H., Dielen, B., 1992. Interference galloping-investigations concerning the phase lag of the flow switching. J. Wind Eng. Ind. Aerod. 43, 2047–2056.
Sarpkaya, T., 2004. A critical review of the intrinsic nature of vortex-induced vibrations. J. Fluid Struct. 19, 389–447.
Skop, R.A., Balasubramanian, S., 1997. A new twist on an old model for vortex-excited vibrations. J. Fluid Struct. 11, 395–412.
Sui, J., Wang, J.S., Liang, S.P., Tian, Q.L., 2016. VIV suppression for a large mass-damping cylinder attached with helical strakes. J. Fluid Struct. 62, 125–146.
Sumner, D., 2010. Two circular cylinders in cross-flow: a review. J. Fluid Struct. 26, 849–899.
Wang, E.H., Xiao, Q., Zhu, Q., Incecik, A., 2017. The effect of spacing on the vortex-induced vibrations of two tandem flexible cylinders. Phys. Fluids 29 (7), 077103.
Williamson, C.H.K., Govardhan, R., 2004. Vortex-induced vibrations. Annu. Rev. Fluid Mech. 36, 413–455.
Xu, G., Zhou, Y., 2004. Strouhal numbers in the wake of two inline cylinders. Exp. Fluid 37 (2), 248–256.
Xu, W.H., Ji, C.N., Sun, H., Ding, W., Bernitsas, M.M., 2019. Flow-induced vibration of two elastically mounted tandem cylinders in cross-flow at subcritical Reynolds numbers. Ocean. Eng. 173, 375–387.
Zdravkovich, M.M., 1974. Flow-induced vibration of two cylinders in tandem arrangements, and their suppression. In: Proceedings of the International Symposium on Flow Induced Structural Vibrations, Karlsruhe 1972, pp. 631–639.
Zdravkovich, M.M., 1987. The effects of interference between circular cylinders in cross flow. J. Fluid Struct. 1 (2), 239–261.
Zdravkovich, M.M., 1988. Review of interference-induced oscillations in flow past two parallel circular cylinders in various arrangements. J. Wind Eng. Ind. Aerod. 28, 183–199.
Zhou, T., Razali, S.M., Hao, Z., Cheng, L., 2011. On the study of vortex-induced vibration of a cylinder with helical strakes. J. Fluid Struct. 27, 903–917.
Zhou, Y., Alam, M.M., 2016. Wake of two interacting circular cylinders: a review. Int. J. Heat Fluid Flow 62, 510–537.
Zhou, Y., Yiu, M.W., 2006. Flow structure, momentum and heat transport in a two tandem-cylinder wake. J. Fluid Mech. 548, 17–48.